



Cell-cell fusion induced by measles virus amplifies the type I interferon response.

Florence Herschke, Sébastien Plumet, Thomas Duhén, Olga Azocar, Johan Druelle, David Laine, Timothy Fabian Wild, Chantal Rabourdin-Combe, Denis Gerlier, Hélène Valentin

► To cite this version:

Florence Herschke, Sébastien Plumet, Thomas Duhén, Olga Azocar, Johan Druelle, et al.. Cell-cell fusion induced by measles virus amplifies the type I interferon response.. *Journal of Virology*, 2007, 81 (23), pp.12859-71. 10.1128/JVI.00078-07 . hal-00169132

HAL Id: hal-00169132

<https://hal.science/hal-00169132>

Submitted on 8 Oct 2008

HAL is a multi-disciplinary open access archive for the deposit and dissemination of scientific research documents, whether they are published or not. The documents may come from teaching and research institutions in France or abroad, or from public or private research centers.

L'archive ouverte pluridisciplinaire **HAL**, est destinée au dépôt et à la diffusion de documents scientifiques de niveau recherche, publiés ou non, émanant des établissements d'enseignement et de recherche français ou étrangers, des laboratoires publics ou privés.

1 **Cell-cell fusion induced by measles virus amplifies the type I interferon**
2 **response**

3
4 F. Herschke^{1‡}, S. Plumet^{1‡}, T. Duhen^{2‡}, O. Azocar², J. Druelle³, D. Laine², T. F. Wild³, C.
5 Rabourdin-Combe^{2\$}, D. Gerlier^{1\$} and H. Valentin^{2\$*}

6
7
8
9 ¹Interactions virus cellule-hôte; CNRS; Université de Lyon 1; FRE3011, IFR 62 Laennec, 69372
10 Lyon Cedex 08 – France

11
12 ²Interaction virus-système immunitaire; INSERM ; U851, IFR128 BioSciences Lyon-Gerland,
13 Université de Lyon 1; 21 Avenue Tony Garnier, 69365 Lyon Cedex 07 – France

14
15 ³Immunobiologie des infections virales; INSERM; U758, IFR128 BioSciences Lyon-Gerland,
16 Université de Lyon 1; 21 Avenue Tony Garnier, 69365 Lyon Cedex 07 – France

17
18 [‡] and ^{\$} These authors equally contributed to this work

19
20 **Running title:** Amplified interferon by virus-induced fusion

21
22 * **Corresponding author:** Phone: (+33) 4 37 28 23 51
23 Fax: (+33) 4 37 28 23 41
24 Mail: valentin@cervi-lyon.inserm.fr

25

26 **Words count for Abstract size:** 246

27 **Words count for Text size (excluding abstract, references and figure legends):** 7184

ACCEPTED

29 **ABSTRACT**

30

31 Measles virus (MeV) infection is characterized by the formation of multinuclear giant cells
 32 (MGC). We report that IFN- β production is amplified *in vitro* by the formation of virus-induced
 33 MGC derived from human epithelial cells or mature conventional dendritic cells (mDC). Both
 34 fusion and IFN- β response amplification was inhibited in a dose dependent way by a fusion
 35 inhibitory peptide after MeV infection of epithelial cells. This effect was observed at both low
 36 and high multiplicity of infection. While in the absence of virus replication, the cell-cell fusion
 37 mediated by MeV H/F glycoproteins did not activate any IFN- α/β production, an amplified IFN-
 38 β response was observed by infecting H/F-induced MGC with a non fusogenic recombinant
 39 chimerical virus. Time-lapse microscopy studies revealed that MeV-infected MGC from
 40 epithelial cells have a highly dynamic behavior and an unexpected long lifespan. Following the
 41 cell-cell fusion, both of the RIG-I and IFN- β gene deficiencies were trans-complemented to
 42 induce an IFN- β production. IFN- β and IFN- α production were also observed in MeV-infected
 43 immature and mature DC (iDC and mDC). In contrast to iDC, MeV infection of mDC induced
 44 MGC which produced enhanced amounts of IFN- α/β . The amplification of IFN- β production
 45 was associated with a sustained nuclear localization of IFN regulatory factor 3 (IRF-3) in MeV-
 46 induced MGC derived from both the epithelial cells and mDC, while the IRF-7 up-regulation was
 47 poorly sensitive to the fusion process. Therefore, MeV-induced cell-cell fusion amplifies IFN-
 48 α/β production in infected cells and this indicates that MGC contribute to the antiviral immune
 49 response.

50 INTRODUCTION

51

52 Measles virus (MeV) is an important human pathogen responsible for ~345 000 of deaths in
53 2005 (<http://www.who.int/mediacentre/factsheets/fs286/en/>). However, most humans clear this
54 viral infection provided that they have a functional cellular and adaptive immunity (19). MeV
55 infection begins in the respiratory tract and then spreads to local lymphoid tissues, where virus
56 replication can occur in macrophages and possibly conventional dendritic cells (cDC) (14, 17, 22,
57 49, 70). This allows MeV spreading to other lymphoid organs and to the whole body. MeV
58 induces a cytopathic effect characterized by the fusion of neighboring cells into multinucleated
59 giant cells (MGC). *In vivo*, seven days after MeV infection of rhesus monkeys, MGC are found in
60 respiratory and genitourinary tract, as well as in the esophagus and skin epithelia (47). In
61 addition, a specific subset of infected MGC called Warthin-Finkeldey cells (WFC), initially
62 described in infants dying of acute measles, is found in primary and secondary lymphoid organs
63 (19). WFC are usually observed in germinal centers and interfollicular areas of secondary
64 lymphoid organs and in the thymus. They are heterogeneous and display either B or T cells
65 markers (54), although macrophage and DC markers have not yet been investigated. *In vitro*,
66 MeV infection of human cells, including primary epithelial cells and cDC, induces the formation
67 of MGC also referred to as syncytia (17, 78, 82). MeV-induced cell-cell fusion is governed by the
68 interaction of the viral envelope H and F glycoproteins with the cellular receptors CD46 and
69 CD150, which are expressed ubiquitously and solely on immune activated cells, respectively
70 (19).

71 The hallmark of the immune response to a viral infection is the rapid production of a range of
72 cytokines, most prominently type I IFN (IFN- α/β). The IFN- α/β enable cells to be protected
73 against viral infection via pleiotropic activities such as inhibition of protein synthesis and cell

74 proliferation, and enhancement of infected cell apoptosis (reviewed in (5, 21)). They also activate
 75 Natural Killer (NK) cells and cytotoxic T cells (CTL) that are capable of eliminating the viral
 76 pathogen by killing infected cells. The IFN- α/β can act directly on CTL or indirectly by inducing
 77 the maturation of cDC, which facilitates cross-presentation of viral antigens to CTL (42, 43). The
 78 single IFN- β gene and most of the IFN- α genes differ in their promoter region, the former is
 79 activated by IFN regulatory factor 3 and 7 (IRF-3/IRF-7) heterodimers (56), whereas only IRF-7
 80 homodimers (25) and/or IRF-7/IRF-8 heterodimers as recently reported in mouse DC (75), can
 81 activate the latter. The recognition of peculiar danger molecular motifs of viruses is mediated by
 82 host pattern recognition receptors (PRR) (36), which can recognize virus nucleic acids. Two
 83 groups of PRR are involved in IFN production in DC, the Toll-like receptors (TLR) and the RIG-
 84 like receptors (RLR). To date, TLR are mainly responsible for IFN- α production by plasmacytoid
 85 DC (pDC) via TLR7 and TLR9 (1), which respond to viral nucleic acids within the endosomal
 86 compartment. Nucleic acid recognition results in the activation of the IFN- α genes through the
 87 phosphorylation and the nuclear translocation of IRF-7 (26, 37). Indeed, in comparison with other
 88 cells, pDC express high level of IRF-7 (8, 30) and this allows pDC to produce 100- to 1000-fold
 89 more IFN- β and IFN- α than other cell types (26). TLR are also involved in IFN production by
 90 cDC via TLR3 after phagocytosis of infected cells (64). However, the IFN response in cDC
 91 principally relies on RLR (RIG-I and MDA-5) (34, 35), which are cytosolic PRR expressed in
 92 almost all nucleated cells and dedicated to respond to viral nucleic acids produced during
 93 replication ((28, 60, 87). MDA-5 and RIG-I recognized dsRNA (20) and 5'-triphosphate ended
 94 RNA (28, 60, 62), respectively. Accordingly, they recognize different types of RNA viruses,
 95 MDA-5 being activated by *Picornaviridae* and RIG-I by *Flaviviridae*, *Orthomyxoviridae* and
 96 *Mononegavirales* (20, 35). MeV activates RIG-I which recognizes the 5'-triphosphate end of the
 97 small RNA leader transcript (62). The activation of RLR induces the interaction with an adaptor

98 protein called IPS-1 (also known as MAVS, VISA, CARDIF) that leads to NF- κ B, IRF-3 and
99 IRF-7 phosphorylation and their transient translocation into the nucleus, resulting in the early
100 IFN- β gene induction (34, 57). In contrast to the short-living IRF-7, the more stable IRF-3 is
101 highly expressed in all cells (25). IFN- β is then secreted and binds to the IFNAR to produce late
102 IFN- β and all IFN- α subtypes. Indeed, early IFN- β induces the transcription of numerous genes
103 known as IFN-stimulated genes (ISG) (25), including IRF-7. The activation of this supplemental
104 source of IRF-7 allows the delayed production of a boost of both IFN- β and IFN- α , according to
105 a robust positive feedback loop, which amplifies the antiviral response (25). The crucial role of
106 the RLR in the IFN- α/β response and control of viral replication has been recently highlighted in
107 IPS-1 (or MAVS) deficient mice, which show normal IFN- α secretion by pDC (41, 74).

108 In the case of MeV, IFN- α/β production has been found after *in vitro* infection of various
109 human cell types including epithelial (from various tissues), endothelial, glial and PBMC (52, 84,
110 85). MeV propagates more efficiently in mature cDC (mDC) than in immature cDC (iDC) and
111 induces higher level of MGC formation in mDC (17, 66). Given the ability of MeV to induce
112 MGC formation in epithelium and secondary lymphoid organs, we aimed at investigating, both in
113 human epithelial cells and cDC, the role of MeV-induced cell-cell fusion on the regulation of
114 IFN- α/β production.

116 **MATERIALS AND METHODS**

117

118 **Reagents.** Antibodies used were: mAbs clone 55 (anti-H), clone 25, and 120 (anti-N), G28.5
119 (anti-CD40) and rabbit polyclonal anti-human IRF-3. The following reagents were used: Hoechst
120 33342 (Sigma), fusion-inhibiting peptide FIP Z-D-Phe-L-Phe-Gly-OH (Neosystem), rhGM-CSF
121 and rhIL-4 (generously provided by Schering-Plough), rhIFN- β (Calbiochem, San Diego, CA),
122 Draq5 (Alexis Biolabs).

123

124 **Cells and phenotypic analysis.** Human kidney epithelial 293T/17 cells (ATCC) expressing
125 CD46 (293T/CD46⁺), HeLa cells, African green monkey Vero fibroblasts (ATCC),
126 293T/CD150⁺ (77), Huh7.5 cells, a subline of Huh7 defective in RIG-I (73), and human cortical
127 TEC (P1.4D6 clone) from postnatal thymus (16) were maintained in DMEM medium
128 supplemented with 10 % FCS or as described in (16, 73). Monocyte-derived DC were generated
129 *in vitro* from human blood (Etablissement de Transfusion Sanguine, Lyon, France) as previously
130 described (17). After 6 days of culture in 200 ng/ml rhGM-CSF and 10 ng/ml rhIL-4, >95% of
131 the cells were iDC. The mDC were derived by treating iDC for 48 h with 10 μ g/ml of mAb anti-
132 CD40. The cDC phenotyping was determined as previously described (17, 82).

133

134 **MeV infection.** MeV (Hallé strain) and recombinant chimerical MGv (72) were maintained
135 in Vero cells. For MeV infection experiments, cells were seeded overnight at appropriate density
136 in a 24-well plate according to the duration of the observation to avoid cell crowding. 293T and
137 TEC were infected at MOI of 1, unless otherwise indicated, then treated or not with FIP. DC
138 were infected at MOI of 0.1 with MeV as previously detailed (17, 83). As controls, all cells were

139 pulsed with a mock preparation corresponding to uninfected Vero cell supernatant. In some
 140 experiments, FIP (100 µg/ml) was added to the cDC cultures infected or not with MeV.

141

142 **Transient cell transfections.** 4×10^5 293T/CD46⁺ cells were plated on 6-well plates (BD,
 143 Falcon). The day after, cells were transfected either with 1 µg pCXN2-F (expressing Edm-F) plus
 144 1 µg pCXN2-EdH (expressing the CD46-binding H^{Ed}) or 1 µg pCXN2-KAH (expressing the H^{KA}
 145 from the wild type KA MeV isolate which does not bind to CD46) (79), or 2 µg of pBSK⁺ carrier
 146 plasmid (Stratagene). All transfections were performed using Lipofectamine (Invitrogen) or
 147 Dreamfect (OZ Biosciences) according to manufacturers' instructions.

148

149 **Time-Lapse.** 2×10^6 293T/CD46⁺ cells were plated on a 6-well plate and infected with MeV
 150 at MOI of 1 as described above. After 24 h of culture in the presence of 10 µg/ml FIP, FIP was
 151 removed and the plate was placed on a 37°C heated in 5% CO₂ atmosphere (Carl Zeiss, Jena,
 152 Germany). Cells were imaged by Metamorph software v6 with a Coolsnap HQ monochrome
 153 camera associated to timelapse microscope (Axiovert 100 M) and a x10 (numerical aperture 0.25)
 154 Plan-Apochromat objective (Zeiss). Meta Imaging Series 4.5 (Universal Imaging, West Chester,
 155 PA) was used to make Quick-Time movies from image stacks from metamorph software. One
 156 picture was made every 10 min for 60 hours and every second of movie represent 235.4 min
 157 (3.92 h) of culture (see Fig. S5video.mov). Images extracted from stacks were processed with
 158 Adobe Photoshop 6.0 (Adobe Systems, San Jose, CA).

159

160 **Co-culture experiments.** 8×10^4 Huh7.5 and Vero cells were plated in 24-well plates
 161 (Costar) and were infected, 24 h later, with MeV at MOI of 1. At 8 h.p.i., Vero cells were
 162 trypsinized and added to the Huh7.5 cell monolayers at a 1:1 ratio, in the presence or absence of

163 10 µg/ml of FIP. Cell-free supernatants were harvested at different times and frozen before
164 analysis for IFN- α/β using a biological assay.

165

166 **IFN- α and IFN- β detection assay.** IFN- α/β contents in supernatants were determined using
167 a bioassay as detailed elsewhere (84). IFN- α and IFN- β were determined by ELISA using the
168 IFN-alpha kit from Bender MedSystems (detection limit = 8 pg/ml), and the IFN-beta kit from
169 PBL Laboratories (detection limit = 250 pg/ml), respectively.

170

171 **RNA extraction, cDNA RT, and real-time QPCR analysis.** A detailed procedure can be
172 found for viral RNA quantification in (61). Primer sets for human IFN- β and IRF-7 mRNA
173 quantitation were forward TGGGAGGATTCTGCATTACC, and reverse
174 CAGCATCTGCTGGTTGAAGA primers, respectively. The primer sets were purchased from
175 Search-LC (Heidelberg, Germany). Results were normalized according to the amounts of 18S
176 rRNA, and expressed in mRNA copy number / 25 ng of total RNA.

177

178 **MTT colorimetric bioassay.** 4×10^3 293T/CD46⁺ cells were plated in a 96-well plate
179 (Costar). At 30 h after infection or transfection, cells were treated with 225 ng/well of 3-(4,5-
180 dimethyl-2-thiazolyl)-2,5-diphenyl-2H-tetrazolium bromide (MTT, Sigma) to measure
181 mitochondrial activity of metabolically active cells. 4 h later, the supernatant was removed and
182 the cells were lysed with 100 µl/well DMSO containing 0.04 N HCl. Absorbance was then
183 measured at 490 and 650 nm (18).

184

Quantitative fusion assay. This assay is based on the conditional expression of β -galactosidase (β -Gal) under the control of the T7 polymerase promoter and was performed as previously described (7).

Subcellular localization of GFP-IRF-3 proteins. 5×10^4 293T/CD46⁺ cells, seeded in 24 well plate were infected or not with MeV at MOI of 1 for 2 h then transfected by the GFP-IRF-3 expression plasmid (46) using lipofectamine. 24 to 48 h latter, GFP-fluorescence in living cells was analyzed with a Leica DM IRB microscope at a magnification of x400. The percent of IRF-3-labeled nuclear was calculated by counting, within a microscope field, the total number of nuclei (belonging to mononuclear cells or MGCs, labeled and unlabeled,) and the number of nuclei labeled with GFP-IRF-3. In each condition, >100 nuclei were counted.

Stainings. For nuclear staining, cell monolayers were stained with Hoechst 33342 as detailed previously (82) and the stained nuclei were observed using a Leica DM IRB microscope.

MeV H cell surface expression was detected using cl55 mAb plus goat anti-mouse IgG phycoerythrin-conjugated secondary antibody (GAM-PE), (Jackson ImmunoResearch Laboratories) as previously described (82). MeV N intracellular detection was performed using Cytofix/Cytoperm kit (Becton Dickinson, Parmingen) and 293T/CD46⁺ cells were labeled using biotinylated cl25 mAb plus streptavidin-PE (Caltag Laboratories) as previously described (82). After labelling, cells were analyzed using a FACScalibur flow cytometer (Becton Dickinson Cellquest software). Integrated fluorescence was measured, and data were collected from at least 5,000 events.

Triple stainings were performed to visualized GFP-IRF-3 (green), MeV N protein (red) and nuclei (blue) by confocal microscopy assays. 2.5×10^4 293T/CD46⁺ cells were seeded onto pre-

209 coated poly-L-Lysine (Sigma, 10 µg/ml, overnight at 4°C) glass coverslips in a 24-well plates
 210 and incubated 20 min at 37°C. 12 h later, cells were infected with MeV at a MOI of 0.1, 1, 2 and
 211 4, followed by transfection of the GFP-IRF-3 expression plasmid as described above, and then
 212 cultured in the absence or the presence of FIP at 10µg/ml. 48 h later, cells were fixed in 2%
 213 paraformaldehyde/PBS for 20 min at room temperature, treated with 0.1% Glycine/PBS for 10
 214 min at room temperature, and permeabilized with 0.5% Triton X-100/PBS for 5 min at room
 215 temperature. After washes with PBS, the fixed cells were blocked in BSA, human and goat
 216 serums, Triton X-100/PBS overnight at +4°C. Cells were then incubated with cl120 anti-N mAb
 217 for 90 min at +4°C. Cells were washed 3 times for 5 min in PBS before incubation with a GAM-
 218 Alexa 568 for 30 min at +4°C. After 3 washes in PBS, cells were mounted on glass slides with
 219 mounting medium (Dako) containing Draq5 as nuclear marker. Labeled cells were imaged with a
 220 confocal microscope (Zeiss LSM510, 1 µm) using a zoomed (x2) 63X (NA 1.4) PlanFluor
 221 objective. To prevent cross-contamination between fluorochromes, each channel was imaged
 222 sequentially using a multi-track recording module before merging.

223 Double staining was performed to visualize endogenous IRF-3 (green) and nuclei (blue) by
 224 Axioplan2 Imaging microscopy assays. Briefly, 8×10^4 mDC were seeded onto pre-coated poly-L-
 225 Lysine glass coverslips in a 24-well plates and incubated 20 min at 37°C. 24h later, cells were
 226 infected at a MOI of 0.1, and then cultured in the absence or the presence of FIP at 100µg/ml. At
 227 3 d.p.i., cells were then fixed as for triple staining. Then, the fixed cells were blocked in
 228 BSA/serums/Triton X-100/PBS for 1 h at +4°C and incubated with rabbit anti-IRF-3 serum for 1
 229 h at +4°C. Cells were washed 3 times for 5 min in PBS before incubation with a goat anti-rabbit
 230 IgG Alexa 488-conjugated secondary antibody (Molecular Probes) for 30 min at +4°C. After 3
 231 washes in PBS, cells were incubated with 1 µg/ml of Hoechst 33343 for 15 min at room
 232 temperature before mounted on glass slides with mounting medium (Dako). Labelled cells were

233 analyzed with an Axioplan2 Imaging microscope (Zeiss, 0.3 μ m) and then imaged by metamorph
234 software V6. Images extracted from Z stacks were processed with Adobe Photoshop 6.0
235 software.

236

237 RESULTS

238 **MeV-induced cell-cell fusion amplifies IFN- β activation in epithelial cells.** While MeV
239 induced a high number of syncytia containing numerous nuclei in cells expressing both MeV
240 receptors (293T/CD46⁺CD150⁺), syncytia were smallest and less numerous in 293T/CD46⁺ cells
241 expressing only CD46 (not shown). MeV infection of 293T/CD46⁺ cells led to the accumulation
242 of F viral transcripts and to the induction of IFN- β gene expression (data not shown). The
243 accumulation of viral F mRNA and the transcription of the IFN- β gene were both enhanced in
244 293T/CD46⁺CD150⁺ cells, compared to 293T/CD46⁺ cells (data not shown). Thus, the level of
245 IFN- β activation was correlated to the virus transcription and/or to the cytopathic effects.

246 To decipher how each of these could influence the IFN response, we took advantage of the
247 availability of a fusion inhibitory peptide (FIP). FIP efficiently blocks the MeV-induced syncytia
248 formation without inhibiting the cell-to-cell virus spreading (19). Addition of FIP repressed both
249 syncytium formation and IFN- α/β production in MeV-infected 293T/CD46⁺ culture, without
250 affecting the proportion of cells expressing MeV-N protein (Fig. 1A, left histogram). Whereas the
251 fusion was totally inhibited by FIP, the IFN- α/β production by day 3 (not shown) and 7 p.i. (Fig.
252 1A, left histogram) was inhibited by ~85-96%. This residual IFN- α/β production was significant,
253 since no IFN- β could be detected in uninfected cells (data not shown). However, 293T cells
254 expressing only MeV-Ed-H and -F glycoproteins readily fused into MGC, but did not secrete any

255 detectable IFN- α/β (data not shown). This indicates that cell-cell fusion, *per se*, does not activate
256 the IFN- α/β response.

257 A recombinant chimerical virus, MGCV, where H and F genes have been substituted by that of
258 the VSV G glycoprotein (72), infected and propagated more slowly in 293T/CD46⁺ cells without
259 inducing syncytium formation. Accordingly, it induced a low level of IFN- β production which
260 was insensitive to FIP (Fig. 1A, right histogram), and equivalent to that observed in FIP-treated
261 MeV-infected 293T/CD46⁺ cells. Thus, MGCV only triggered a basal level of IFN- α/β response,
262 in agreement with the observation of the low IFN- α/β inducing ability of a non-fusogenic MeV
263 variant (48). To confirm the enhancing effect of cell-cell fusion on MeV-induced IFN- β response,
264 we compared the effect of expressing *in trans* a fusing (H^{Ed}F) and a non fusing (H^{KA}F) (79)
265 glycoprotein combination on the IFN- β response induced by MGCV infection. As expected, the
266 expression of H^{KA}F did affect neither virus nor IFN- β transcription (not shown). In contrast,
267 when compared to H^{KA}F, the expression of H^{Ed}F induced large syncytia into 293T/CD46⁺ cells, a
268 minor increase of viral transcription and a significant increase in the IFN- β gene activation (Fig.
269 1B). Furthermore, the enhancing effect on the IFN- β response was much more pronounced in
270 conditions ensuring that every single got infected, i.e. at MOI of 4, with a ~25 fold enhancement
271 of IFN- β mRNA accumulation, compared to a limited 2.5 fold increase in virus transcript
272 accumulation.

273 When 293T/CD46⁺ cells were infected with fusogenic MeV at MOI ranging from 0.01 up to
274 4 and analyzed at 30 h.p.i., the viral transcription of the F messenger exhibited a dose-response
275 curve between MOI of 0.01 and 1 then reached a plateau (Fig. 1C, upper histograms). The
276 identical level of viral transcription between MOI of 1 and 4 suggested that some viral
277 interference occurred. In addition, at MOI higher than 1, a cytotoxicity, increasing with the MOI
278 used, was observed, that likely resulted in part from cell fusion from without (i.e. fusion between

adjacent cells bridged by viral particles) (6), a reminder of viral induced hemolysis of CD46 expressing Vervet monkey red blood cells (59). Furthermore, syncytia formation was much reduced when compared to lower MOI likely because of the strong down-regulation of CD46 upon contact with the large amount of the hemagglutinin brought about by the high viral inoculum (39, 51). The level of IFN- β transcription followed the same dose-response between MOI of 0.01 and 1, to reach a plateau at MOI of 1, 2 and 4 (Fig. 1C, middle histograms). This correlation between viral transcription and IFN- β gene activation agrees with their parallel kinetics observed at MOI of 1 (62). Surprisingly, the production of IFN- α/β in the supernatant measured at 3 d.p.i. was almost identical between MOI of 0.1 and 4 (Fig. 1C, lower histograms). At MOI of 0.01, a small amount of IFN- α/β was detected only later at 7 d.p.i. (data not shown). The addition of FIP, which inhibited the formation of syncytia at all MOI (Fig. 1C), had minimal effects on viral transcription, but strongly inhibited IFN- β gene transcription and protein secretion (Fig. 1C, black columns), except at MOI of 4. Interestingly, in the presence of FIP, the amount of IFN released in the supernatant and the MOI correlated for MOI between 0.1 and 2 (Fig. 1C and data not shown). At MOI of 0.01, the level of IFN released detected at 7 d.p.i. was also inhibited by FIP (not shown). The lack of FIP inhibitory effect at MOI of 4 was likely reflecting the side effects of the too high viral load mentioned above.

Furthermore, after infection at MOI of 1, FIP inhibition of the cell-cell fusion observed at 30 h.p.i. and 3 d.p.i., was dose-dependent as assessed by nucleus staining with Hoechst 33342 (Fig. 2A, and data not shown), and the quantification assay using β -Gal as a reporter gene for intercellular fusion (Fig. 2B). A similar inhibition curve was also observed for the IFN- β mRNA (Fig. 2C and not shown). Strikingly, the best mathematical equation describing these two dose-dependent responses had similar slopes (-11) and ordinates at the origin (+42 and +39).

302 In summary, MeV replication triggers a basal IFN- β response independently of H/F proteins
 303 and MeV-induced cell-cell fusion robustly amplifies this response in a dose-dependent manner at
 304 both low and high MOI.

305

306 **High morphologic plasticity of MeV-induced MGC.** Viral induced fusion is usually
 307 correlated with apoptosis (13). As we observed an increased synthesis of IFN- β in MGC, we
 308 further analyzed the morphological plasticity of these cells. Thirty hours p.i., syncytia were found
 309 to be metabolically active, and able to convert MTT into intracellular formazan crystals, a
 310 hallmark of mitochondrial activity in viable epithelial cells (data not shown).

311 Studies by time-lapse microscopy over 60 hours of MeV-infected 293T/CD46⁺ cells, showed
 312 the syncytia to be dynamic, exhibiting a morphology which varied with time (Fig. 3A, B and Fig.
 313 S3Avideo.mov). In the 1st stage, the initial flat adherent syncytium increased in size and nucleus
 314 contents (Fig. 3A, Adherent). Dynamic pseudopodia emerged from the syncytium to contact
 315 surrounding cells or syncytia. In a 2nd stage, the adherent syncytium retracted into highly
 316 refringent smooth balls (3rd stage), where nuclei were no longer visible, except upon examination
 317 under confocal microscopy of z-stacks after Hoechst staining (see below). Balls were highly
 318 mobile and rolled around. When they encountered surrounding healthy adherent mononuclear
 319 cells, they spread out into a secondary flat adherent syncytium with visible nuclei (4th stage).
 320 Then, the secondary adherent syncytium retracted again (5th stage), into an irregular ball with
 321 protruding blisters giving them a cauliflower appearance (6th stage), which rolled around. The
 322 duration of each stage was highly variable (see mean values on Fig. 3B), and most of the initial
 323 syncytia passed through stages 1, 2 and 3, half of them passed through stages 4 and 5 to reach
 324 stage 6, and another half directly passed from stage 3 to stage 6 (Fig. 3B). Of 17 initial syncytia
 325 recorded during 3 different experiments, none appeared to die before 60 hours. Furthermore,

when individual smooth or blistered balls were transferred onto a fresh uninfected 293T/CD46⁺ monolayer, they re-adhered. This suggests that syncytia may have an indefinite lifespan provided that they find within their vicinity a healthy cell monolayer (Fig. 3B, and data not shown). In contrast, when transferred to a plastic dish covered or not by collagen, both smooth and blistered balls became senescent and finally died to become floating and optically clear bubble-like structures (data not shown). Thus, MeV-induced syncytia are not prone to quickly die; instead, they may remain a viable entity. As controls, cell-to-cell fusion was observed neither in uninfected nor in FIP-treated MeV-infected 293T/CD46⁺ cells, indicating that none of the observed syncytium was due to merging senescent 293T/CD46⁺ cells (Fig. 3C and data not shown).

336

Cell-cell fusion brings together both danger activation signal and IFN- β gene to trigger IFN- β induction. We then studied whether MeV-induced fusion can trigger trans-complementation using Huh7.5 cells and Vero cells which have disabled RIG-I (73) and lack the IFN- β gene (11, 12), respectively. IFN- α/β was secreted and accumulated over time from both of the MeV-Huh7.5/Vero and MeV-Vero/Huh7.5 cell co-culture combinations, as syncytia were observed (Fig. 4). Moreover, the addition of FIP completely blocked both of the cellular fusion and the IFN- α/β production to undetectable levels. As expected, MeV infection of isolated Huh7.5 or Vero cells induced syncytia but did not trigger any IFN- α/β response. Thus, the RIG-I defect in human Huh7.5 cells and IFN- β gene defect in the simian Vero cells could be trans-complemented in fused cells allowing the triggering of the human IFN- β gene.

347

IRF-7 expression level is not influenced by MeV-induced fusion in epithelial cells. We then investigated whether the enhancement of IFN- β gene expression mediated by MeV-induced

cell-cell fusion correlate with the up-regulation of IRF-7. To this end, the level of IRF-7 transcripts was analyzed in 293T/CD46⁺ cells and in the primary thymic epithelial cells (TEC), which are IFNAR-competent, in the presence or the absence of FIP (Fig. 5). In both of these cell types, MeV infection resulted in the activation of the IFN- β and IRF-7 genes. However, the level of IRF-7 transcripts remained unchanged when syncytia formation was blocked by FIP treatment, and did not correlate with the IFN- β mRNA level. Thus, the amplification of IFN- β activation by MeV-induced cell-cell fusion is not directly or solely controlled by the level of IRF-7 expression.

MeV-induced cell-cell fusion amplifies IFN- α and IFN- β responses in human mDC, but not iDC. The phenomenon of the amplification of the IFN- α/β response by MeV-induced cell-cell fusion was then examined in human monocyte-derived DC. More than 95% of iDC and mDC were CD1a⁺ and CD14⁺ (data not shown). While the immature phenotype was confirmed by the low or negative expression of MHC class II, CD83, CD40, CD80 and CD86, mDC expressed high level of these molecules (data not shown). In agreement with previous reports (17, 50), both iDC and mDC, which have a CD46⁺CD150^{Low} and CD46⁺CD150^{High} phenotype, respectively (Fig. 6A) (50), were sensitive to MeV infection as shown by MeV-F transcription (Fig. 6B). However, the sensitivity to infection differed between iDC and mDC. MeV replication was faster in mDC in comparison with iDC with ~230-fold higher transcription at 3 d.p.i. (Fig. 6B). While the iDC only poorly fused, the MeV-infected mDC contained numerous giant MGC (Fig. 6), which expressed both viral proteins and mDC markers ((17), and data not shown). The addition of FIP to the cDC did not significantly affect the MeV-F transcription in the iDC and only partially reduced the MeV-F transcription in the mDC (Fig. 6B), while FIP efficiently inhibited the formation of MGC (Fig. 6). We then investigated the IFN- α/β production in cDC following MeV infection. MeV-infected iDC secreted significant levels of bioactive IFN- α/β (Fig. 6C) and

374 IFN- α (Fig. 6D). No IFN- β production was detected (Fig. 6E), even though IFN- β transcripts
 375 were observed (Fig. 6F), because of either the limited sensitivity of the ELISA, or the
 376 consumption of IFN- β by MeV-infected iDC (25). According to the very low level of cell-cell
 377 fusion observed within MeV infected iDC, the addition of FIP did not affect the IFN- α/β
 378 production (Fig. 6C and D). The MeV infected mDC produced significant levels of bioactive
 379 IFN- α/β , IFN- α , and IFN- β (Fig. 6C-E) and IFN- β mRNA (Fig. 6F). Both the MGC formation
 380 and IFN- α/β production by MeV-infected mDC was strongly inhibited in the presence of FIP
 381 (Fig. 6C-F). Thus, the MeV infection induces IFN- α/β responses in both of the iDC and mDC.
 382 However, the virus-induced cell-cell fusion amplifies both the IFN- α and IFN- β production only
 383 in mDC. Interestingly, MeV infection induced an IRF-7 up-regulation in the iDC, but not in mDC
 384 (Fig. 6G). Furthermore, FIP did not significantly affect the expression of IRF-7 in both DC types
 385 (Fig. 6G).

386 As a control, the non fusigenic chimerical virus MGCV was also used to infect iDC and
 387 mDC. MGCV only induced, in both iDC and mDC, a basal IFN response, which was not sensitive
 388 to FIP (data not shown). We noticed that, contrary to MeV, MGCV replicated better in iDC than in
 389 mDC (Fig. 6A) and, accordingly, induced a stronger IFN- β gene transcription in iDCs. We
 390 speculate that the stronger endocytosis ability of iDC over mDC can favor MGCV entry, which
 391 relies on the acidic endosomal pathway mediated by the VSV-G glycoprotein.

392 Thus, MeV infection induces IFN- α/β responses in both iDC and mDC. However, the virus-
 393 induced cell-cell fusion amplifies both IFN- α and IFN- β production only in mDC.

394

395 **Sustained nuclear translocation of IRF-3 in MeV-induced MGC derived from epithelial**
 396 **cells and mDC.** MeV infection induces transactivation of the IFN- β gene through the
 397 phosphorylation and nuclear translocation of IRF-3 (65). Therefore, we analyzed the changes in

the subcellular IRF-3 localization using a GFP-tagged IRF-3 (GFP-IRF-3) transfected into 293T/CD46⁺ cells. As expected (46), the GFP-IRF-3 was localized exclusively within the cytoplasm of uninfected cells (Fig. 7A, mock). After MeV infection, nuclei from a single syncytium exhibited a diverse level of GFP-IRF-3 staining, thus looking asynchronous, and a large proportion of syncytia contained nuclear IRF-3 whichever their stage. In addition, few mononuclear MeV-infected cells surrounding outside MGCs displayed nuclear localization of GFP-IRF-3 (not shown). In the absence of FIP, 50±24% of the nuclei belonging to MGC were labeled with GFP-IRF-3, whereas, only 6±7% of the small amount of single cells, which remained outside MGC, had their nuclei labelled (Fig. 7A, MeV). In the presence of FIP, although most cells were infected (see Fig. 1A, 7B and S7B), nuclear translocation of GFP-IRF-3 was observed only in 4±2% of them (Fig. 7A, MeV+FIP, $2\alpha=0.01$ when compared to 50±24 % of nucleus labelling in the absence of FIP. In all cases, the nuclei were intact, including those in syncytia, as shown by Hoescht staining (Fig. 7A).

Confocal analysis of GFP-IRF3 distribution in 293T/CD46⁺ cells infected with MeV at MOI of 1 and 2 confirmed the high rate of nuclear IRF-3 labeling in MGC compared to mononuclear cells, and the presence of cytoplasmic N protein in all but rare cells, (data not shown). At the lower MOI of 0.1, similar results were obtained. Upon confocal analysis, many nuclei within MGC were labeled with GFP-IRF-3, whereas GFP-IRF-3 remained excluded from the nuclei of non infected cells (Fig. 7B, and data not shown). When the fusion was prevented by the addition of FIP, only few mononuclear cell nuclei displayed GFP-IRF3 labelling, although most of them were clearly infected as shown by cytoplasmic N labeling (Fig. 7B red dots and patches, and data not shown). Again, GFP-IRF-3 was translocated into the nuclei of MGC at all stages of the adherent-ball cycle described in Fig. 3 (Fig. 7B and data not shown). Interestingly, the distribution of both N and GFP-IRF-3 tended to change with the morphological stage of the MGC. When the syncytium was flat and adherent, GFP-IRF-3 showed dotted and/or reticulated

423 distribution in the nuclei and N protein had a dotted cytoplasmic distribution. When the
 424 syncytium underwent retraction into a smooth ball, the intensity of the nuclear GFP-IRF-3
 425 labeling became stronger and more diffuse and N protein tend to aggregate further into larger
 426 patches at the periphery of the cytoplasm (Fig. 7B, and data not shown). Thus, the amplification
 427 of IFN- β production induced by MeV-mediated fusion correlates with a sustained and strong
 428 nuclear translocation of IRF-3 within MGC at all their morphological stages.

429 Localization of endogenous IRF-3 during infection of mDC was also studied. As expected,
 430 endogenous IRF-3 distributed exclusively within the cytoplasm of uninfected mDC (Fig. 7C,
 431 mock, left panels). At 3 d.p.i., IRF-3 (green) staining of many intact nuclei (blue stain) in
 432 syncytia MeV-infected mDC was observed (Fig. 7C, right panels, and supplemental material Fig.
 433 S7Cvideo.mov). Interestingly, the distribution of endogenous IRF-3 in the nuclei of mDC-
 434 derived syncytia looked very similar to that of GFP-IRF-3 in nuclei of 293T-derived syncytia
 435 (compare Fig. 7C with 7A, B and data not shown). Addition of FIP strongly inhibited both MeV-
 436 infected MGC from mDC and nuclear localization of endogenous IRF-3 (Fig. 7C, middle panel).
 437 Thus, endogenous IRF-3 tended to remain translocated into nuclei within MGC from MeV-
 438 infected mDC in agreement with the sustained nuclear translocation of exogenous GFP-IRF-3
 439 within MGC derived from epithelial cells.

440

441 **DISCUSSION**

442

443 We report here that MeV-induced MGC or syncytia derived from epithelial cells and
 444 mDCs are metabolically active, long living and display both sustained nuclear translocation of
 445 IRF-3 and enhanced activation of the IFN- β gene. (i) There is a correlation between the fusogenic
 446 activity of MeV strain and IFN- β production. (ii) The fusion enhancing effect is observed at both

447 low and high MOI. (iii) The fusion inhibitory peptide FIP inhibits, in a dose dependent manner,
 448 both cell-cell fusion and IFN- β production. (iv) Cell-cell fusion mediated by MeV-H and -F
 449 glycoproteins does not activate any IFN- β response in the absence of viral infection, but does it
 450 after infection with MGCV, a non-fusiogenic chimerical virus. (v) The cytosolic PRR RIG-I and
 451 the IFN- β gene are trans-complemented during the fusion process. (vi) Although both iDC and
 452 mDC are infected by MeV, only mDC undergo massive cell-cell fusion. In the mDC, a robust
 453 IFN- α/β production is mediated by MeV-induced cell-cell fusion (vii) In both epithelial cells and
 454 mDC, the fusion enhancing effect on IFN- β response appears to be mediated by a sustained
 455 nuclear IRF-3 localization, but does not directly correlate with the up-regulation of IRF-7
 456 expression. (viii) In response to MeV, iDC also produces an IFN- α/β production, but it is
 457 independent of the fusion process and likely amplified via IRF-7. Altogether, our results indicate
 458 that the MeV-induced MGC in epithelial cells and mDC are important sources of IFN- α/β and
 459 that the fusion can mediate an enhancement of IFN- α/β production without modulating the
 460 expression of IRF-7.

461 Cell-cell fusion is a hallmark of many viral infections, and resulting MGC were thought to
 462 be short lived. Indeed, syncytia induced by the HIV-1 glycoprotein died by apoptosis by at least
 463 three different mechanisms: transient lipid exchange, activation of several kinases and
 464 transcription factors and contagious apoptosis (58). Surprisingly, MeV-induced MGC from
 465 epithelial cells were found to be viable and dynamic entities, capable of transducing intracellular
 466 signals throughout their morphological stage changes. Thus, from our *in vitro* observations, we
 467 can predict that the physiopathological MGC (WFC) observed in lymph nodes and thymus from
 468 MeV-infected children and primates should have a rather long lifespan *in vivo* (54, 76). However,
 469 as described by us and others (13, 58, 63, 82), syncytium apoptosis finally occurs, probably
 470 depending on cellular environment deprivation.

471 In non-pathological situations, the contents of a cell nucleus should be tightly regulated to
 472 ensure that every cell harbors a single nucleus. Notable exceptions are the fusion of cellular
 473 precursors undergoing a specific maturation process, such as the myotubes, the osteoclasts, and
 474 the syncytiotrophoblasts. In the two latter cases, a survival program is turned on (15, 31).
 475 Whether such a mechanism occurs for the survival of MeV-induced MGC remains to be
 476 determined. Strikingly, both of the MeV-induced MGC and syncytiotrophoblasts need to recruit
 477 fresh mononuclear cells in order to survive (29). Furthermore, given that IFN- β is used as a retro-
 478 control feedback to limit the size of the osteoclasts by preventing further recruitment of new
 479 mononuclear cells (9), it could also regulate the dynamics of MGC formation induced by MeV as
 480 observed for other viruses (53, 80, 81, 86).

481 The MeV induced cell-cell fusion results in MGC harboring an important function in the
 482 innate immunity, and it could be questioned if the fusion *per se* acts as an activation signal.
 483 Indeed, the artificial fusion of a human cell line with chicken erythrocytes results in the activation
 484 of both human and chicken IFN- β (23), the latter being indicative of a reactivation of the dormant
 485 chicken erythrocyte nucleus. The MeV induced cell-cell fusion is mediated by the H binding to
 486 the CD46 or CD150 cellular receptor which results in the activation of the fusion F protein (19).
 487 The H binding to CD46 has been reported to activate the IFN- β response and NO $^{\bullet}$ production in
 488 murine macrophages expressing human CD46 (33). In human epithelial cells, the H/F and CD46-
 489 mediated fusion *per se* was unable to trigger the IFN- β response, which required virus
 490 transcription (62). Likewise, we can exclude that the interaction of H with TLR2 is involved in
 491 the IFN- β activation since (i) the signaling downstream to TLR2 occurred independently of the F
 492 glycoprotein, (ii) the use of a wild type MeV with H protein unable to bind to CD46 and TLR2
 493 (4) gave similar results (not shown), and (iii) the TLR2 signaling pathway is not linked to IFN-

494 α/β production. Altogether, MeV-induced cell-cell fusion in human epithelial cells is not directly
495 sensed as a danger signal by the innate cellular machinery.

496 MeV infection of human epithelial cells triggers the production of IFN- β , which is
497 differentially regulated in mononuclear cells and MGC. At the beginning of the viral infection,
498 the activation of IFN- β occurs in MeV-infected mononuclear cells where the cytosolic RIG-I is
499 activated upon recognition of the 5'-tri-phosphate end of MeV leader RNA (62), and this results
500 in the activation of IRF-3. Then, IRF-3 undergoes phosphorylation, homo- or hetero-
501 dimerization, nuclear translocation, fixation on IFN sensitive responsive elements (ISRE) and
502 degradation by the ubiquitin-proteasome pathway (3, 65). In a later phase, the amplification of
503 IFN- β production in MeV-infected mononuclear epithelial cells can be mediated by the classical
504 IFNAR/IRF-7-dependent positive feedback, as described for other viruses (27), since IRF-7 is
505 up-regulated after MeV infection. In contrast, the robust IFN- β production mediated by MGC
506 from epithelial cells could not be explained solely by the IRF-7 up-regulation, because the latter
507 was poorly sensitive to the fusion process. As described for an infection with respiratory
508 syncytial virus, IRF-3 nuclear translocation occurs early within few hours after infection, then it
509 drops rapidly within 15 hours because of the anti-interferon activity of non structural proteins
510 (71). Therefore, the presence of a high IRF-3 nuclear translocation within MGC at a late time (30
511 h.p.i.) of the MeV infection is unexpected and supports an essential role of IRF-3 in the MGC-
512 mediated amplification of the IFN- β production. It is possible that MeV proteins with IFN
513 antagonist activity are diluted out upon fusion of MGC with uninfected cells, thus allowing a
514 stronger and more sustained IFN production. It remains to be determined if the sustained IRF-3
515 nuclear localization within MGC occurs as phosphorylated IRF-3 homodimers or IRF-3/IRF-7
516 heterodimers.

517 What could be the mechanism, which enables cell fusion to boost the IFN- β activation ?
518 At low MOI (virus to cell ratio <1) of infection, we propose the following model. Since the RIG-I
519 and IFN- β gene locus are trans-complemented during the cell-cell fusion, syncytia formation can
520 boost IFN- β transcription by bringing uninfected cells into contact with viral PAMPs. At a given
521 time, the level of IFN- β activation results from the balance between available trigger viral RNA
522 (PAMPs), RIG-I (PRR), pathway components (i.e. IRF-3) and viral IFN antagonists. The
523 sustained nuclear localization of IRF-3 in the nuclei within syncytia at low MOI is compatible
524 with the continuous recruitment of non infected cells which can result either in a weaken
525 concentration of viral antagonists, and/or the recruitment of “naive” RIG-I/pathway components
526 molecules by MeV leader RNA which would be produced in excess over the amount of RIG-
527 I/pathway components available in a single cell. At high MOI, an alternative model should be
528 made since all individual cells get infected prior to the fusion event and the fusion-mediated
529 amplification of the IFN- β response is even higher (see Fig. 1B). The IRF-3 nuclear translocation
530 could be sustained within MeV-induced MGC, because of a synergistic activity such as
531 stabilization of phosphorylated IRF-3 by activation of the DNA-dependent protein kinase (DNA-
532 PK) (32). This will require further investigations. Presently, our data thus argue for two non
533 exclusive mechanisms involved in the fusion enhancing effect on IFN- β activation, one,
534 evidenced at low MOI, is the recruitment of non infected cells to MeV-infected MGC, and the
535 other, at high MOI, is a synergistic effect of cell fusion and virus infection. In both cases, there is
536 a sustained nuclear translocation of IRF-3 within MGC, the underlying mechanism of which
537 remains to be more deeply examined. In every case, the amplification of IFN- β response by MGC
538 derived from MeV-infected epithelial cells upgrades the alert level of the innate immune response
539 against viral infection in peripheral tissues.

540 During natural infection, MeV infects lung epithelial cells and/or resident iDC in epithelia
 541 and mucosa, and likely induces local IFN- α/β production, which could limit MeV replication
 542 (45). Then, infected iDC can migrate and disseminate the virus to the draining lymph nodes.
 543 There, they can be stimulated via CD40L by encountering naive T lymphocytes and become
 544 activated and more permissive to MeV replication as shown experimentally (66). Because the
 545 mDC are prone to fuse with surrounding cells, they form MGC, which could correspond to the
 546 WFC found in lymphoid organs. This results in a high virus progeny, which can propagate
 547 throughout the body. There are several examples of IFN- α/β production by human or mouse iDC
 548 (2, 34, 35) infected *in vitro* by few viruses, including MeV (38). Here, we demonstrate that upon
 549 MeV infection, both of the iDC and mDC produce IFN- β and IFN- α *in vitro*. The iDC display
 550 low permissiveness to MeV infection, and rapidly produce high levels of IFN- α and IFN- β
 551 independently of cell-cell fusion, probably through IFNAR/IRF-7 signaling as judged by the up-
 552 regulation of IRF-7 expression. Since, IFN- α/β is quickly produced and secreted by iDC after
 553 infection with MeV (not shown), IFN- α/β can protect cells against the propagation of MeV and
 554 strongly limit the formation of MGC. As iDC are present in peripheral tissues and secrete IFN-
 555 α/β , they can contribute to the establishment of the innate antiviral state by enhancing
 556 cytotoxicity of NK cells and activating macrophages (10, 40). In addition, the iDC constitute a
 557 critical link between innate and adaptive immunity (44, 67). Indeed, the IFN- α/β induce the up-
 558 regulation of co-stimulatory molecules CD80, CD86 and CD40 on cDC (24), and the expression
 559 of TRAIL on iDC, which become cytotoxic (83). Thus, the IFN- α/β produced by MeV-infected
 560 iDC is a signal which upgrades the alarm level of the cellular innate immunity for detecting the
 561 invasion of a possible pathogen.

562 In contrast to the iDC, the mDC are highly susceptible to MeV infection, form large MGC
 563 and produce high levels of IFN- α/β . The IFN- α/β is therefore less efficient in limiting MeV

564 growth and MGC formation within the mDC than within the iDC. The opposite phenotypes of
 565 iDC and mDC could originate from different relative kinetics of the infection and the innate
 566 antiviral response. Indeed, when the strength of the initial activation of IFN- β is too low
 567 compared to the virus growth kinetics, the rapid accumulation of MeV encoded anti-IFN α/β and
 568 possibly C proteins can block the intracellular IFNAR signaling pathway (55, 69), and this paves
 569 the way for unlimited virus growth. We therefore favor that the MGC can be promoted or
 570 repressed according to the respective speed and strength of virus growth and IFN- α/β production.
 571 Upon infection, the mDC produce IFN- α/β mostly from MGC, without any IRF-7 up-regulation.
 572 This suggests that the IFNAR/IRF-7 feedback loop is not directly involved. This data is in
 573 agreement with the down-regulation of IFNAR in cDC upon their maturation (68). As for
 574 epithelial cells, the robust production of IFN- α/β by the MeV-mediated MGC from mDC also
 575 correlated with a sustained activation of IRF-3. However, the induction of IFN- α independently
 576 of IRF-7 up-regulation in the MGC is questionable and the mechanism remains to be determined.
 577 The IFN- α/β produced by MGC from MeV-infected mDC could rather be involved in the
 578 establishment of MeV-specific adaptive immune response in the secondary lymph nodes. By
 579 providing high viral antigen load and IFN- α/β -dependent enhancement of the cross-priming to T
 580 cells (43), the paradoxical accumulation of virus and IFN- α/β within the MeV-mediated MGC
 581 probably contributes to the stimulation of the MeV-specific adaptive immune response, which
 582 will finally clear the virus from the organism. Finally, because of the different abilities of various
 583 laboratory, vaccine and wild type MeV to counteract the cellular innate immunity, the virus strain
 584 dependency of cell fusion-mediated amplification of the IFN- α/β response is also currently under
 585 investigation.

586

587 **ACKNOWLEDGMENTS**

589 We thank Drs C. Servet for helpful discussions, and C. Chamontin, C. Bella, F. Simian-Lermé
 590 and C. Lionnet (Flow cytometry and PLATIM platforms of IFR128) for their helpful technical
 591 assistance. This work benefited from the technical facilities of the CeCIL platform of IFR62. This
 592 work would not having been possible without mAbs, plasmids, recombinant virus and/or cell
 593 lines kindly provided by M. Billeter, C. Rice, M. L. Toribio, K. Takeuchi, A Garcia-Sastre, J.
 594 Hiscott, Y. Yanagi, E. Berger, and Schering-Plough (Dardilly, France). This work was supported
 595 in part by grants from ANR (DG, ANR-MIME), INSERM, INCA-Canceropole 2004-2005 and
 596 ARC 3637. D.L., F.H., J.D., T.D., and S.P. were supported by a fellowship from MENRT, ARC
 597 and DGA, respectively. The authors have no conflicting financial interests.

598

599

600 REFERENCES

601

1. **Asselin-Paturel, C., G. Brizard, K. Chemin, A. Boonstra, A. O'Garra, A. Vicari, and G. Trinchieri.** 2005. Type I interferon dependence of plasmacytoid dendritic cell activation and migration. *J Exp Med* **201**:1157-67.
2. **Barchet, W., A. Krug, M. Cella, C. Newby, J. A. Fischer, A. Dzionek, A. Pekosz, and M. Colonna.** 2005. Dendritic cells respond to influenza virus through TLR7- and PKR-independent pathways. *Eur J Immunol* **35**:236-42.
3. **Bibeau-Poirier, A., S. P. Gravel, J. F. Clement, S. Rolland, G. Rodier, P. Coulombe, J. Hiscott, N. Grandvaux, S. Meloche, and M. J. Servant.** 2006. Involvement of the IkappaB kinase (IKK)-related kinases tank-binding kinase 1/IKKi and cullin-based ubiquitin ligases in IFN regulatory factor-3 degradation. *J Immunol* **177**:5059-67.

4. **Bieback, K., E. Lien, I. M. Klagge, E. Avota, J. Schneider-Schaulies, W. P. Duprex, H. Wagner, C. J. Kirschning, V. Ter Meulen, and S. Schneider-Schaulies.** 2002. Hemagglutinin protein of wild-type measles virus activates toll-like receptor 2 signaling. *J Virol* **76**:8729-36.
5. **Bonjardim, C. A.** 2005. Interferons (IFNs) are key cytokines in both innate and adaptive antiviral immune responses--and viruses counteract IFN action. *Microbes Infect* **7**:569-78.
6. **Bratt, M. A., and W. R. Gallaher.** 1969. Preliminary analysis of the requirement for fusion from within and from without by Newcastle disease virus. *Proc. Natl. Acad. Sci. USA* **64**:537-543.
7. **Christiansen, D., P. Devaux, B. Reveil, A. Evlashev, B. Horvat, J. Lamy, C. Rabourdin-Combe, J. H. Cohen, and D. Gerlier.** 2000. Octamerization enables soluble CD46 receptor to neutralize measles virus in vitro and in vivo. *J Virol* **74**:4672-8.
8. **Coccia, E. M., M. Severa, E. Giacomini, D. Monneron, M. E. Remoli, I. Julkunen, M. Cella, R. Lande, and G. Uze.** 2004. Viral infection and Toll-like receptor agonists induce a differential expression of type I and lambda interferons in human plasmacytoid and monocyte-derived dendritic cells. *Eur J Immunol* **34**:796-805.
9. **Coelho, L. F., G. Magno de Freitas Almeida, F. J. Mennechet, A. Blangy, and G. Uze.** 2005. Interferon-alpha and -beta differentially regulate osteoclastogenesis: role of differential induction of chemokine CXCL11 expression. *Proc Natl Acad Sci U S A* **102**:11917-22.
10. **Dalod, M., T. Hamilton, R. Salomon, T. P. Salazar-Mather, S. C. Henry, J. D. Hamilton, and C. A. Biron.** 2003. Dendritic cell responses to early murine cytomegalovirus infection: subset functional specialization and differential regulation by interferon alpha/beta. *J Exp Med* **197**:885-98.

11. **Diaz, M. O., S. Ziemin, M. M. Le Beau, P. Pitha, S. D. Smith, R. R. Chilcote, and J. D. Rowley.** 1988. Homozygous deletion of the alpha- and beta 1-interferon genes in human leukemia and derived cell lines. *Proc Natl Acad Sci U S A* **85**:5259-63.
12. **Emeny, J. M., and M. J. Morgan.** 1979. Regulation of the interferon system: evidence that Vero cells have a genetic defect in interferon production. *J Gen Virol* **43**:247-52.
13. **Esolen, L. M., S. W. Park, J. M. Hardwick, and D. E. Griffin.** 1995. Apoptosis as a cause of death in measles virus-infected cells. *J Virol* **69**:3955-8.
14. **Esolen, L. M., B. J. Ward, T. R. Moench, and D. E. Griffin.** 1993. Infection of monocytes during measles. *J Infect Dis* **168**:47-52.
15. **Feng, X.** 2005. Regulatory roles and molecular signaling of TNF family members in osteoclasts. *Gene* **350**:1-13.
16. **Fernandez, E., A. Vicente, A. Zapata, B. Brera, J. J. Lozano, C. Martinez, and M. L. Toribio.** 1994. Establishment and characterization of cloned human thymic epithelial cell lines. Analysis of adhesion molecule expression and cytokine production. *Blood* **83**:3245-54.
17. **Fugier-Vivier, I., C. Servet-Delprat, P. Rivaller, M. C. Rissoan, Y. J. Liu, and C. Rabourdin-Combe.** 1997. Measles virus suppresses cell-mediated immunity by interfering with the survival and functions of dendritic and T cells. *J Exp Med* **186**:813-23.
18. **Gerlier, D., and N. Thomasset.** 1986. Use of MTT colorimetric assay to measure cell activation. *J Immunol Methods* **94**:57-63.
19. **Gerlier, D., H. Valentin, D. Laine, C. Rabourdin-Combe, and C. Servet-Delprat.** 2006. Subversion of the immune system by measles virus: a model for the intricate interplay between a virus and the human immune system, p. 225-292. *In* P. J. Lachman

and M. B. A. Oldstone (ed.), Microbial Subversion of Host Immunity. Caister Academic Press, Norwalk, UK.

20. **Gitlin, L., W. Barchet, S. Gilfillan, M. Cella, B. Beutler, R. A. Flavell, M. S. Diamond, and M. Colonna.** 2006. Essential role of mda-5 in type I IFN responses to polyriboinosinic:polyribocytidylic acid and encephalomyocarditis picornavirus. *Proc Natl Acad Sci U S A* **103**:8459-64.
21. **Goodbourn, S., L. Didcock, and R. E. Randall.** 2000. Interferons: cell signalling, immune modulation, antiviral response and virus countermeasures. *J Gen Virol* **81**:2341-64.
22. **Grosjean, I., C. Caux, C. Bella, I. Berger, F. Wild, J. Banchereau, and D. Kaiserlian.** 1997. Measles virus infects human dendritic cells and blocks their allostimulatory properties for CD4+ T cells. *J Exp Med* **186**:801-12.
23. **Guggenheim, M. A., R. M. Friedman, and A. S. Rabson.** 1968. Interferon: production by chick erythrocytes activated by cell fusion. *Science* **159**:542-3.
24. **Honda, K., S. Sakaguchi, C. Nakajima, A. Watanabe, H. Yanai, M. Matsumoto, T. Ohteki, T. Kaisho, A. Takaoka, S. Akira, T. Seya, and T. Taniguchi.** 2003. Selective contribution of IFN-alpha/beta signaling to the maturation of dendritic cells induced by double-stranded RNA or viral infection. *Proc Natl Acad Sci U S A* **100**:10872-7.
25. **Honda, K., A. Takaoka, and T. Taniguchi.** 2006. Type I interferon [correction of inteferon] gene induction by the interferon regulatory factor family of transcription factors. *Immunity* **25**:349-60.
26. **Honda, K., H. Yanai, T. Mizutani, H. Negishi, N. Shimada, N. Suzuki, Y. Ohba, A. Takaoka, W. C. Yeh, and T. Taniguchi.** 2004. Role of a transductional-transcriptional processor complex involving MyD88 and IRF-7 in Toll-like receptor signaling. *Proc Natl Acad Sci U S A* **101**:15416-21.

27. **Honda, K., H. Yanai, H. Negishi, M. Asagiri, M. Sato, T. Mizutani, N. Shimada, Y. Ohba, A. Takaoka, N. Yoshida, and T. Taniguchi.** 2005. IRF-7 is the master regulator of type-I interferon-dependent immune responses. *Nature* **434**:772-7.
28. **Hornung, V., J. Ellegast, S. Kim, K. Brzozka, A. Jung, H. Kato, H. Poeck, S. Akira, K. K. Conzelmann, M. Schlee, S. Endres, and G. Hartmann.** 2006. 5'-Triphosphate RNA is the ligand for RIG-I. *Science* **314**:994-7.
29. **Huppertz, B., C. Bartz, and M. Kokozidou.** 2006. Trophoblast fusion: fusogenic proteins, syncytins and ADAMs, and other prerequisites for syncytial fusion. *Micron* **37**:509-17.
30. **Izaguirre, A., B. J. Barnes, S. Amrute, W. S. Yeow, N. Megjugorac, J. Dai, D. Feng, E. Chung, P. M. Pitha, and P. Fitzgerald-Bocarsly.** 2003. Comparative analysis of IRF and IFN- α expression in human plasmacytoid and monocyte-derived dendritic cells. *J Leukoc Biol* **74**:1125-38.
31. **Jurisicova, A., J. Detmar, and I. Caniggia.** 2005. Molecular mechanisms of trophoblast survival: from implantation to birth. *Birth Defects Res C Embryo Today* **75**:262-80.
32. **Karpova, A. Y., M. Trost, J. M. Murray, L. C. Cantley, and P. M. Howley.** 2002. Interferon regulatory factor-3 is an in vivo target of DNA-PK. *Proc Natl Acad Sci U S A* **99**:2818-23.
33. **Katayama, Y., A. Hirano, and T. C. Wong.** 2000. Human receptor for measles virus (CD46) enhances nitric oxide production and restricts virus replication in mouse macrophages by modulating production of α/β interferon. *J Virol* **74**:1252-7.
34. **Kato, H., S. Sato, M. Yoneyama, M. Yamamoto, S. Uematsu, K. Matsui, T. Tsujimura, K. Takeda, T. Fujita, O. Takeuchi, and S. Akira.** 2005. Cell type-specific involvement of RIG-I in antiviral response. *Immunity* **23**:19-28.

35. **Kato, H., O. Takeuchi, S. Sato, M. Yoneyama, M. Yamamoto, K. Matsui, S. Uematsu, A. Jung, T. Kawai, K. J. Ishii, O. Yamaguchi, K. Otsu, T. Tsujimura, C. S. Koh, C. Reis e Sousa, Y. Matsuura, T. Fujita, and S. Akira.** 2006. Differential roles of MDA5 and RIG-I helicases in the recognition of RNA viruses. *Nature* **441**:101-5.
36. **Kawai, T., and S. Akira.** 2006. Innate immune recognition of viral infection. *Nat Immunol* **7**:131-7.
37. **Kawai, T., S. Sato, K. J. Ishii, C. Coban, H. Hemmi, M. Yamamoto, K. Terai, M. Matsuda, J. Inoue, S. Uematsu, O. Takeuchi, and S. Akira.** 2004. Interferon-alpha induction through Toll-like receptors involves a direct interaction of IRF7 with MyD88 and TRAF6. *Nat Immunol* **5**:1061-8.
38. **Klagge, I. M., V. ter Meulen, and S. Schneider-Schaulies.** 2000. Measles virus-induced promotion of dendritic cell maturation by soluble mediators does not overcome the immunosuppressive activity of viral glycoproteins on the cell surface. *Eur J Immunol* **30**:2741-50.
39. **Krantic, S., C. Gimenez, and C. Roubardin-Combe.** 1995. Cell-to-cell contact via measles virus haemagglutinin-CD46 interaction triggers CD46 downregulation. *J. Gen. Virol.* **76**:2793-2800.
40. **Krug, A., A. R. French, W. Barchet, J. A. Fischer, A. Dzionek, J. T. Pingel, M. M. Orihuela, S. Akira, W. M. Yokoyama, and M. Colonna.** 2004. TLR9-dependent recognition of MCMV by IPC and DC generates coordinated cytokine responses that activate antiviral NK cell function. *Immunity* **21**:107-19.
41. **Kumar, H., T. Kawai, H. Kato, S. Sato, K. Takahashi, C. Coban, M. Yamamoto, S. Uematsu, K. J. Ishii, O. Takeuchi, and S. Akira.** 2006. Essential role of IPS-1 in innate immune responses against RNA viruses. *J Exp Med* **203**:1795-803.

42. **Lapenta, C., S. M. Santini, M. Spada, S. Donati, F. Urbani, D. Accapezzato, D. Franceschini, M. Andreotti, V. Barnaba, and F. Belardelli.** 2006. IFN- α -conditioned dendritic cells are highly efficient in inducing cross-priming CD8(+) T cells against exogenous viral antigens. *Eur J Immunol* **36**:2046-60.
43. **Le Bon, A., N. Etchart, C. Rossmann, M. Ashton, S. Hou, D. Gewert, P. Borrow, and D. F. Tough.** 2003. Cross-priming of CD8+ T cells stimulated by virus-induced type I interferon. *Nat Immunol* **4**:1009-15.
44. **Le Bon, A., and D. F. Tough.** 2002. Links between innate and adaptive immunity via type I interferon. *Curr Opin Immunol* **14**:432-6.
45. **Leopardi, R., T. Hyypia, and R. Vainionpaa.** 1992. Effect of interferon- α on measles virus replication in human peripheral blood mononuclear cells. *Apmis* **100**:125-31.
46. **Lin, R., C. Heylbroeck, P. M. Pitha, and J. Hiscott.** 1998. Virus-dependent phosphorylation of the IRF-3 transcription factor regulates nuclear translocation, transactivation potential, and proteasome-mediated degradation. *Mol Cell Biol* **18**:2986-96.
47. **McChesney, M. B., C. J. Miller, P. A. Rota, Y. D. Zhu, L. Antipa, N. W. Lerche, R. Ahmed, and W. J. Bellini.** 1997. Experimental measles. I. Pathogenesis in the normal and the immunized host. *Virology* **233**:74-84.
48. **McCullough, K. C.** 1983. Characterization of a non-syncytiogenic autonomously replicating variant of measles virus. *J Gen Virol* **64 Pt 3**:749-54.
49. **Mrkic, B., B. Odermatt, M. A. Klein, M. A. Billeter, J. Pavlovic, and R. Cattaneo.** 2000. Lymphatic dissemination and comparative pathology of recombinant measles viruses in genetically modified mice. *J Virol* **74**:1364-72.

50. **Murabayashi, N., M. Kurita-Taniguchi, M. Ayata, M. Matsumoto, H. Ogura, and T. Seya.** 2002. Susceptibility of human dendritic cells (DCs) to measles virus (MV) depends on their activation stages in conjunction with the level of CDw150: role of Toll stimulators in DC maturation and MV amplification. *Microbes Infect* **4**:785-94.
51. **Naniche, D., T. F. Wild, C. Rabourdin-Combe, and D. Gerlier.** 1993. Measles virus haemagglutinin induces down-regulation of gp57/67, a molecule involved in virus binding. *J. Gen. Virol.* **74**:1073-1079.
52. **Naniche, D., A. Yeh, D. Eto, M. Manchester, R. M. Friedman, and M. B. Oldstone.** 2000. Evasion of host defenses by measles virus: wild-type measles virus infection interferes with induction of Alpha/Beta interferon production. *J Virol* **74**:7478-84.
53. **Nishida, J., H. Yoshikura, T. Okabe, A. Urabe, and F. Takaku.** 1985. Interferons inhibit syncytia-forming ability and in vitro transmission of human T-cell leukemia virus. *Jpn J Cancer Res* **76**:249-52.
54. **Nozawa, Y., N. Ono, M. Abe, H. Sakuma, and H. Wakasa.** 1994. An immunohistochemical study of Warthin-Finkeldey cells in measles. *Pathol Int* **44**:442-7.
55. **Ohno, S., N. Ono, M. Takeda, K. Takeuchi, and Y. Yanagi.** 2004. Dissection of measles virus V protein in relation to its ability to block alpha/beta interferon signal transduction. *J Gen Virol* **85**:2991-9.
56. **Panne, D., T. Maniatis, and S. C. Harrison.** 2007. An Atomic Model of the Interferon-beta Enhanceosome. *Cell* **129**:1111-23.
57. **Paz, S., Q. Sun, P. Nakhaei, R. Romieu-Mourez, D. Goubau, I. Julkunen, R. Lin, and J. Hiscott.** 2006. Induction of IRF-3 and IRF-7 phosphorylation following activation of the RIG-I pathway. *Cell Mol Biol (Noisy-le-grand)* **52**:17-28.

58. **Perfettini, J. L., M. Castedo, T. Roumier, K. Andreau, R. Nardacci, M. Piacentini, and G. Kroemer.** 2005. Mechanisms of apoptosis induction by the HIV-1 envelope. *Cell Death Differ* **12 Suppl 1**:916-23.
59. **Peries, J. R., and C. Chany.** 1960. [Hemagglutinating and hemolytic activity of the measles virus.]. *C R Hebd Seances Acad Sci* **251**:820-1.
60. **Pichlmair, A., O. Schulz, C. P. Tan, T. I. Naslund, P. Liljestrom, F. Weber, and C. Reis e Sousa.** 2006. RIG-I-mediated antiviral responses to single-stranded RNA bearing 5'-phosphates. *Science* **314**:997-1001.
61. **Plumet, S., and D. Gerlier.** 2005. Optimized SYBR green real-time PCR assay to quantify the absolute copy number of measles virus RNAs using gene specific primers. *J Virol Methods* **128**:79-87.
62. **Plumet, S., F. Herschke, J. M. Bourhis, H. Valentin, S. Longhi, and D. Gerlier.** 2007. Cytosolic 5'-Triphosphate Ended Viral Leader Transcript of Measles Virus as Activator of the RIG I-Mediated Interferon Response. *PLoS ONE* **2**:e279.
63. **Scheller, C., and C. Jassoy.** 2001. Syncytium formation amplifies apoptotic signals: a new view on apoptosis in HIV infection in vitro. *Virology* **282**:48-55.
64. **Schulz, O., S. S. Diebold, M. Chen, T. I. Naslund, M. A. Nolte, L. Alexopoulou, Y. T. Azuma, R. A. Flavell, P. Liljestrom, and C. Reis e Sousa.** 2005. Toll-like receptor 3 promotes cross-priming to virus-infected cells. *Nature* **433**:887-92.
65. **Servant, M. J., B. ten Oever, C. LePage, L. Conti, S. Gessani, I. Julkunen, R. Lin, and J. Hiscott.** 2001. Identification of distinct signaling pathways leading to the phosphorylation of interferon regulatory factor 3. *J Biol Chem* **276**:355-63.
66. **Servet-Delprat, C., P. O. Vidalain, H. Bausinger, S. Manie, F. Le Deist, O. Azocar, D. Hanau, A. Fischer, and C. Rabourdin-Combe.** 2000. Measles virus induces abnormal differentiation of CD40 ligand-activated human dendritic cells. *J Immunol* **164**:1753-60.

67. **Servet-Delprat, C., P. O. Vidalain, H. Valentin, and C. Rabourdin-Combe.** 2003. Measles virus and dendritic cell functions: how specific response cohabits with immunosuppression. *Curr Top Microbiol Immunol* **276**:103-23.
68. **Severa, M., M. E. Remoli, E. Giacomini, J. Ragimbeau, R. Lande, G. Uze, S. Pellegrini, and E. M. Coccia.** 2006. Differential responsiveness to IFN-alpha and IFN-beta of human mature DC through modulation of IFNAR expression. *J Leukoc Biol* **79**:1286-94.
69. **Shaffer, J. A., W. J. Bellini, and P. A. Rota.** 2003. The C protein of measles virus inhibits the type I interferon response. *Virology* **315**:389-97.
70. **Shingai, M., N. Inoue, T. Okuno, M. Okabe, T. Akazawa, Y. Miyamoto, M. Ayata, K. Honda, M. Kurita-Taniguchi, M. Matsumoto, H. Ogura, T. Taniguchi, and T. Seya.** 2005. Wild-type measles virus infection in human CD46/CD150-transgenic mice: CD11c-positive dendritic cells establish systemic viral infection. *J Immunol* **175**:3252-61.
71. **Spann, K. M., K. C. Tran, and P. L. Collins.** 2005. Effects of nonstructural proteins NS1 and NS2 of human respiratory syncytial virus on interferon regulatory factor 3, NF-kappaB, and proinflammatory cytokines. *J Virol* **79**:5353-62.
72. **Spielhofer, P., T. Bachi, T. Fehr, G. Christiansen, R. Cattaneo, K. Kaelin, M. A. Billeter, and H. Y. Naim.** 1998. Chimeric measles viruses with a foreign envelope. *J Virol* **72**:2150-9.
73. **Sumpter, R., Jr., Y. M. Loo, E. Foy, K. Li, M. Yoneyama, T. Fujita, S. M. Lemon, and M. Gale, Jr.** 2005. Regulating intracellular antiviral defense and permissiveness to hepatitis C virus RNA replication through a cellular RNA helicase, RIG-I. *J Virol* **79**:2689-99.

74. **Sun, Q., L. Sun, H. H. Liu, X. Chen, R. B. Seth, J. Forman, and Z. J. Chen.** 2006. The specific and essential role of MAVS in antiviral innate immune responses. *Immunity* **24**:633-42.
75. **Tailor, P., T. Tamura, and K. Ozato.** 2006. IRF family proteins and type I interferon induction in dendritic cells. *Cell Res* **16**:134-40.
76. **Tajima, M., and S. Kudow.** 1976. Morphology of the Warthin-Finkeldey giant cells in monkeys with experimentally induced measles. *Acta Pathol Jpn* **26**:367-80.
77. **Takeda, M., S. Ohno, F. Seki, K. Hashimoto, N. Miyajima, K. Takeuchi, and Y. Yanagi.** 2005. Efficient rescue of measles virus from cloned cDNA using SLAM-expressing Chinese hamster ovary cells. *Virus Res* **108**:161-5.
78. **Takeuchi, K., N. Miyajima, N. Nagata, M. Takeda, and M. Tashiro.** 2003. Wild-type measles virus induces large syncytium formation in primary human small airway epithelial cells by a SLAM(CD150)-independent mechanism. *Virus Res* **94**:11-6.
79. **Tatsuo, H., N. Ono, K. Tanaka, and Y. Yanagi.** 2000. SLAM (CDw150) is a cellular receptor for measles virus. *Nature* **406**:893-7.
80. **Tomita, Y., and T. Kuwata.** 1981. Suppressive effects of interferon on cell fusion by Sendai virus. *J Gen Virol* **55**:289-95.
81. **Tomita, Y., and T. Kuwata.** 1979. Suppressive effects of interferon on syncytium formation by RD-114 virus in human transformed cells. *J Gen Virol* **43**:111-7.
82. **Valentin, H., O. Azocar, B. Horvat, R. Williems, R. Garrone, A. Evlashev, M. L. Toribio, and C. Roubardin-Combe.** 1999. Measles virus infection induces terminal differentiation of human thymic epithelial cells. *J Virol* **73**:2212-21.
83. **Vidalain, P. O., O. Azocar, H. Yagita, C. Roubardin-Combe, and C. Servet-Delprat.** 2001. Cytotoxic activity of human dendritic cells is differentially regulated by double-stranded RNA and CD40 ligand. *J Immunol* **167**:3765-72.

84. **Vidalain, P. O., D. Laine, Y. Zaffran, O. Azocar, C. Servet-Delprat, T. F. Wild, C. Rabourdin-Combe, and H. Valentin.** 2002. Interferons mediate terminal differentiation of human cortical thymic epithelial cells. *J Virol* **76**:6415-24.
85. **Volckaert-Vervliet, G., H. Heremans, M. De Ley, and A. Billiau.** 1978. Interferon induction and action in human lymphoblastoid cells infected with measles virus. *J Gen Virol* **41**:459-66.
86. **Wells, D. E., S. Chatterjee, M. J. Mulligan, and R. W. Compans.** 1991. Inhibition of human immunodeficiency virus type 1-induced cell fusion by recombinant human interferons. *J Virol* **65**:6325-30.
87. **Yoneyama, M., M. Kikuchi, T. Natsukawa, N. Shinobu, T. Imaizumi, M. Miyagishi, K. Taira, S. Akira, and T. Fujita.** 2004. The RNA helicase RIG-I has an essential function in double-stranded RNA-induced innate antiviral responses. *Nat Immunol* **5**:730-7.

602 **FIGURE LEGENDS**

603

604 **Figure 1. Role of cell-cell fusion and MeV infection in the IFN- β response.** (A) Syncytia
 605 formation scored as in Fig. S1, % of cells expressing MeV-N protein determined by flow
 606 cytometry, and IFN- α/β production at 7 d.p.i. after infection of 293T/CD46⁺ cells with MeV (left
 607 histogram), or recombinant chimerical MGCV (right histogram), in the absence (dotted columns)
 608 or presence of 10 μ g/ml of FIP (black columns). (B) Syncytia formation and accumulation of
 609 MeV-N (upper panel) and IFN- β (lower panel) transcripts at 23 h.p.i. in 293T/CD46⁺ cells
 610 transiently expressing H^{Ed}F (grid columns) or H^{KAF} (checked columns), respectively.
 611 293T/CD46⁺ cells were infected with MGCV with different MOI, then they were transfected at 2
 612 h.p.i. (C) Dose response relationship of MeV-F transcription and IFN- β mRNA accumulation at
 613 30 h.p.i. and IFN- α/β secretion at 3 d.p.i. with the MOI of MeV used to infect 293T/CD46⁺ cells
 614 in the absence (dotted columns) or the presence of 10 μ g/ml FIP (black columns). Data are mean
 615 values \pm s.d. from two to three independent experiments. ND: not detected. † indicates cell
 616 cytotoxicity.

617

618 **Figure 2. Similar dose-dependent inhibition of cell-cell fusion and IFN- β gene**
 619 **transcription by FIP.** 293T/CD46⁺ (A and C) or HeLa (B) cells were infected with MeV MOI of
 620 1 prior to the addition of increasing amounts of FIP. (A) Micrographs of adherent cells stained
 621 with Hoechst 33342 (magnification x400) at 72 h.p.i. Cells containing more than three nuclei
 622 were considered as syncytia (white arrows). (B) Dose-dependent inhibition of cell-cell fusion by
 623 FIP quantified by colorimetric β -Gal reporter gene expression assay. (C) Dose-dependent
 624 inhibition of IFN- β mRNA accumulation by FIP at 30 h.p.i. Data are means \pm s.d. of triplicates.

625

626 **Figure 3. MeV-induced syncytia are dynamic entities with extended lifespan.** MeV-
627 infected 293T/CD46⁺ were cultured overnight in the presence of FIP, then cultured in the absence
628 (A, B) or the presence (C) of FIP (10 µg/ml) with recorded imaging for the next 60 h by time-
629 lapse microscopy. Images at a magnification x10 were extracted from Fig. S3Avideo.mov and
630 another video not shown at 12.83 h, 15 h, 16.66 h, 25.33 h, 32.5 h and 35.33 h recorded times.
631 (B) The duration of each stage was evaluated and expressed as mean ± s.d. of 17 microscopic
632 areas from three to four separate experiments. The frequency was estimated and indicated as the
633 proportion (%) that underwent transition through a given stage.

634

635 **Figure 4. Reciprocal trans-complementation of RIG-I and IFN-β deficient cells by**
636 **MeV-induced fusion.** RIG-I-deficient Huh7.5 or IFN-β-deficient Vero cells were infected with
637 MeV at MOI of 1, and co-cultured 8 h later with uninfected Vero and Huh7.5 cells (ratio 1:1),
638 respectively. The co-cultures were treated or not with 10 µg/ml of FIP. Cell-free supernatants
639 were collected at 30 and 60 h.p.i. to measure IFN-α/β production. At the end of the co-culture,
640 the cell monolayers were stained for fluorescent nuclei (magnification of x400) for counting
641 within every syncytium indicated by arrows. Data are from one representative experiment out of
642 two. ND: not detected.

643

644 **Figure 5. Unlike IFN-β gene, IRF-7 gene expression does not correlate with cell-cell**
645 **fusion.** 293T/CD46⁺ cells (left panels) and TEC (right panels) were either treated with 1000
646 IU/ml of rhIFN-β or infected with MeV MOI of 1 and cultured in the absence or presence of FIP
647 (10 µg/ml). Expression of IFN-β (upper dotted histograms) and IRF-7 (lower black histograms)

648 mRNA was quantified at 30 h.p.i. Data are from one representative experiment out of two or
649 three. ND: not detected.

650

651 **Figure 6. Mature, but not immature, DC exhibit fusion-dependent amplification of IFN-**
652 **α and IFN- β responses.** iDC and mDC were mock infected or infected with MeV strain at MOI
653 of 0.1, in the absence (dotted columns) or the presence (black columns) of FIP (100 μ g/ml).
654 Syncytia formation was scored for each condition as described in Fig. S1. (A) CD150 expression
655 on iDC and mDC cultures was analyzed by flow cytometry. (B) MeV-F transcript accumulation
656 in iDC and mDC cultures was measured at 3 d.p.i. (C) Secreted bioactive IFN- α/β in cell-free
657 supernatants collected at 3 d.p.i. IFN- α (D) and IFN- β (E) were measured by ELISA at 3 d.p.i.
658 Accumulation of (F) IFN- β and (G) IRF-7 transcripts at 3 d.p.i. in cDC cultures in the absence or
659 the presence of FIP (100 μ g/ml). Data are mean values from two to five separate experiments.
660 ND: not detected.

661

662 **Figure 7. Nuclear translocation of IRF-3 can be triggered within MeV-induced syncytia.**
663 (A) Nuclear translocation of GFP-IRF-3 within syncytia of 293T/CD46⁺ cells infected by MeV at
664 MOI of 1. Microphotographs (magnification x400) showing morphology (upper panels), Hoescht
665 labeled nuclei (middle panels) and GFP-IRF-3 labeled nuclei (bottom panels) at 30 h.p.i.
666 Micrographs (magnification of x400) of uninfected cells (mock) and cells infected with MeV in
667 the absence (MeV) or the presence of FIP (10 μ g/ml, MeV+FIP) are shown. Data are from one
668 representative experiment out of four. (B) Three-color overlays of confocal images showing the
669 distribution of GFP-IRF-3 (green), N (red), nuclei (Draq5, blue) in 293T/CD46⁺ cells infected or
670 not with MOI of 0.1 MeV in the presence or absence of FIP and transfected with GFP-IRF-3.
671 Syncytium images were taken at three morphological stages, flat adherent, retracting and smooth

672 ball, respectively. The whole set of one-color images used to build the overlays is shown in the
673 supplementary Fig.7SB. (C) Nuclear localization of endogenous IRF-3 in MGC derived from
674 MeV-infected mDC. mDC were mock-treated (left panel, magnification x63) or infected with
675 MeV at a MOI of 0.1 in the absence (middle panel, magnification x40) or the presence (right
676 panel, magnification x63) of FIP (100 µg/ml). 3 d.p.i., mDC culture were stained with anti-IRF-3
677 (green, left panel) and with nucleus staining (Hoechst 33343, blue). Cells were analyzed with an
678 axioplan microscope.

679

680 LEGENDS TO SUPPLEMENTAL DATA

681 **Figure S3Avideo.mov. Time-lapse microscopy of MeV-infected 293T/CD46⁺ in the**
682 **absence of FIP.** Animation Format: 380x331 million; sequence, FPS 3,75; Reading: IPS 9; Flow:
683 9,46 mbits/sec; Duration: 9,26 sec; Size and actual size: 100%: 338x331 pixels (see material and
684 methods and legends to Figure 3 for details).

685

686 **Figure S7Cvideo.mov. Nuclear endogenous IRF3 localisation within MeV-induced**
687 **MGC from mDC.** z stack compilation of images from MeV-infected mDC in the absence of FIP
688 (see material and methods).

689

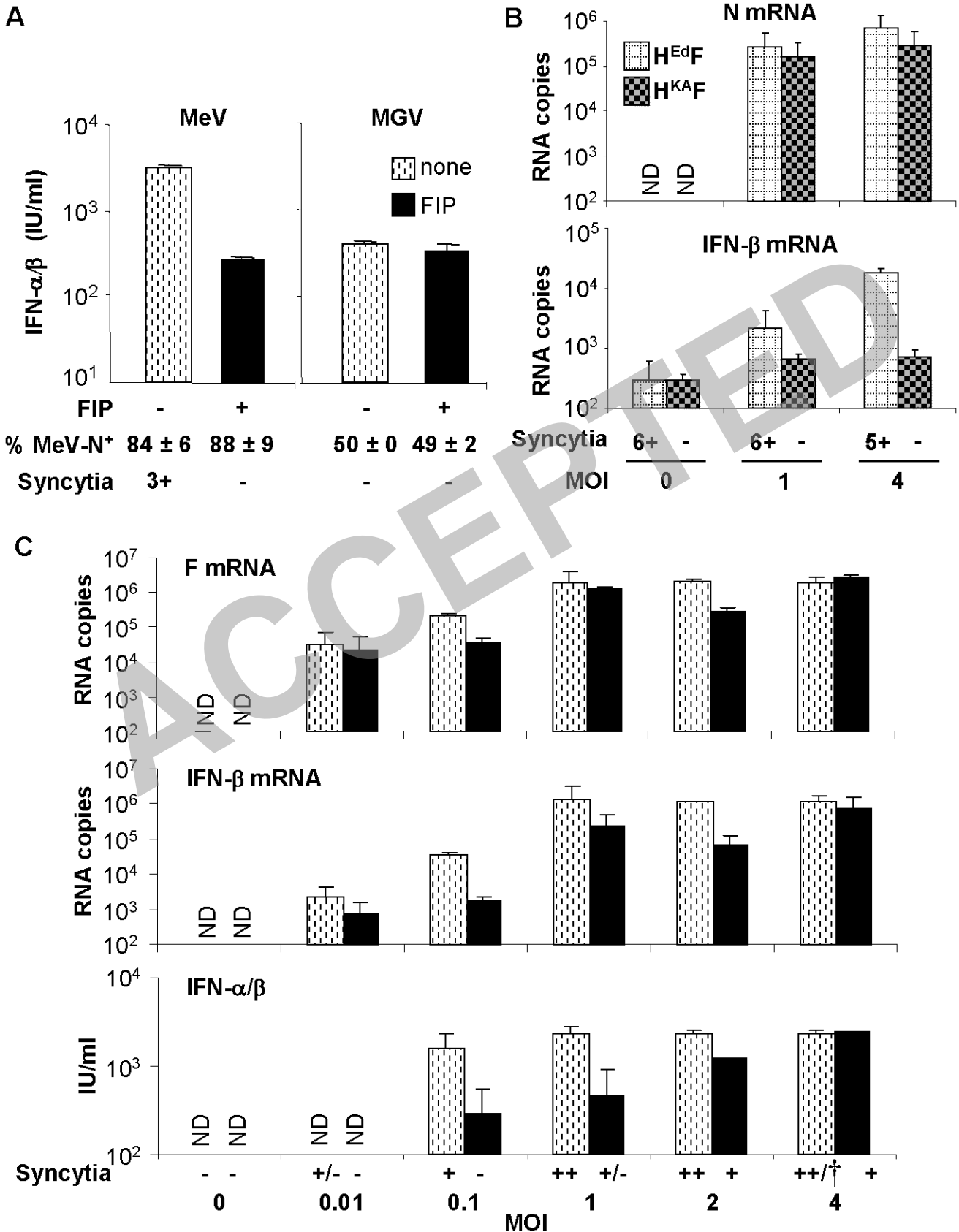
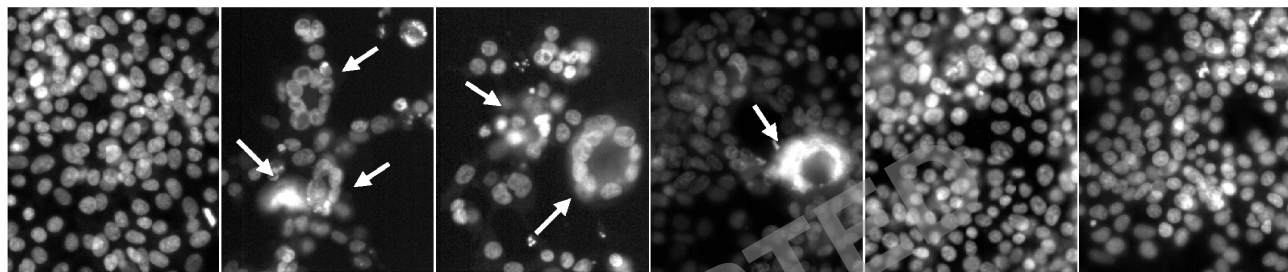
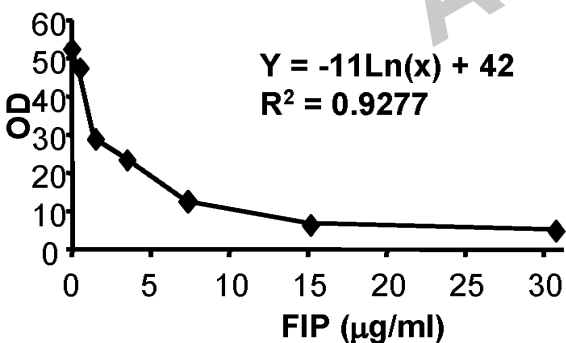
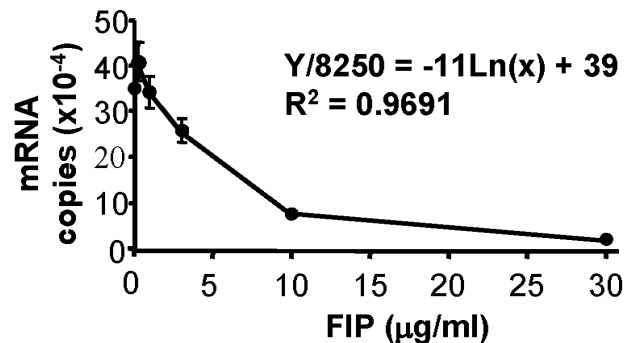


Figure 1

A

MeV:	-	+	+	+	+	+
FIP:	0	0	1 $\mu\text{g/ml}$	3 $\mu\text{g/ml}$	10 $\mu\text{g/ml}$	30 $\mu\text{g/ml}$

B**Fusion****C****IFN- β** *Figure 2*

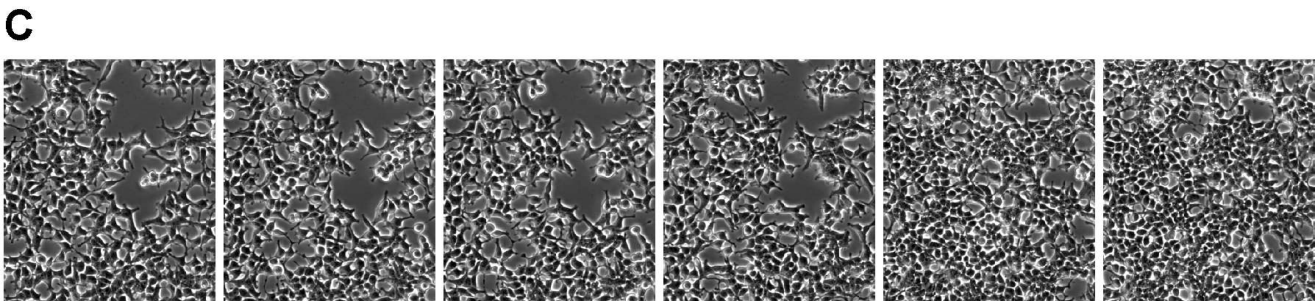
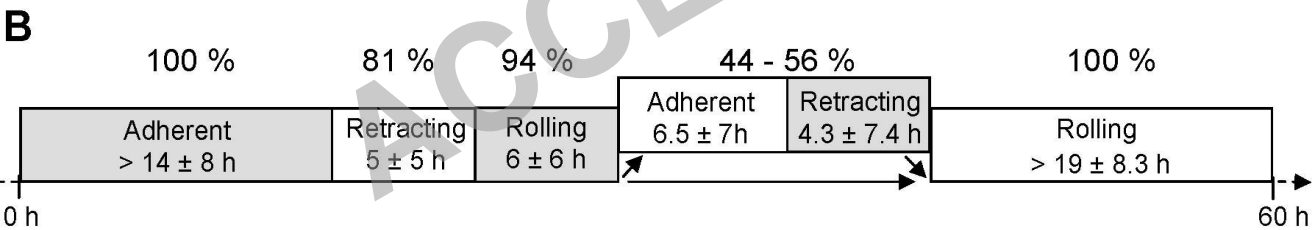
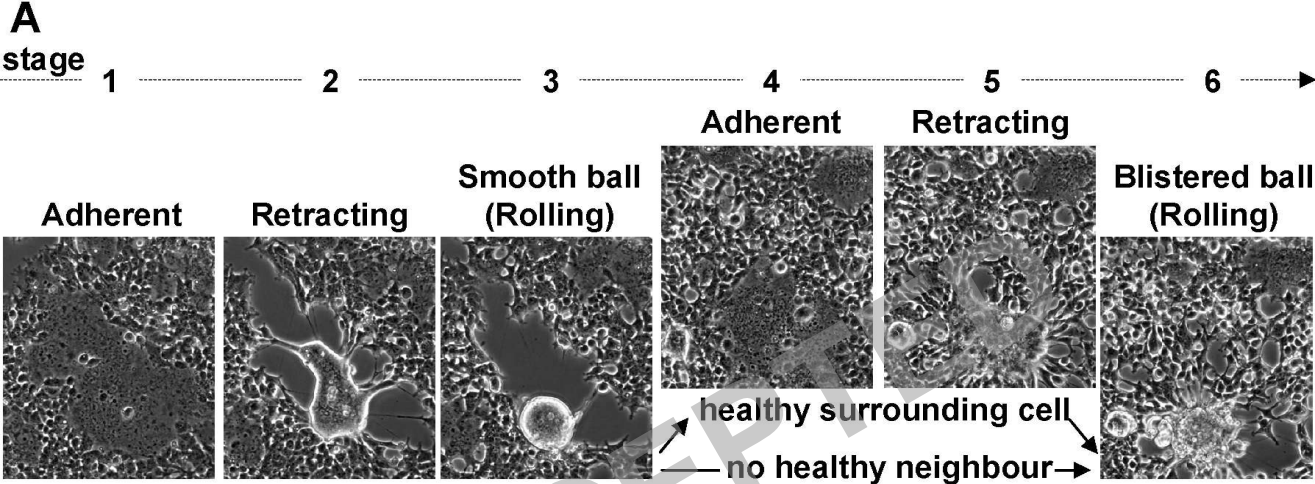


Figure 3

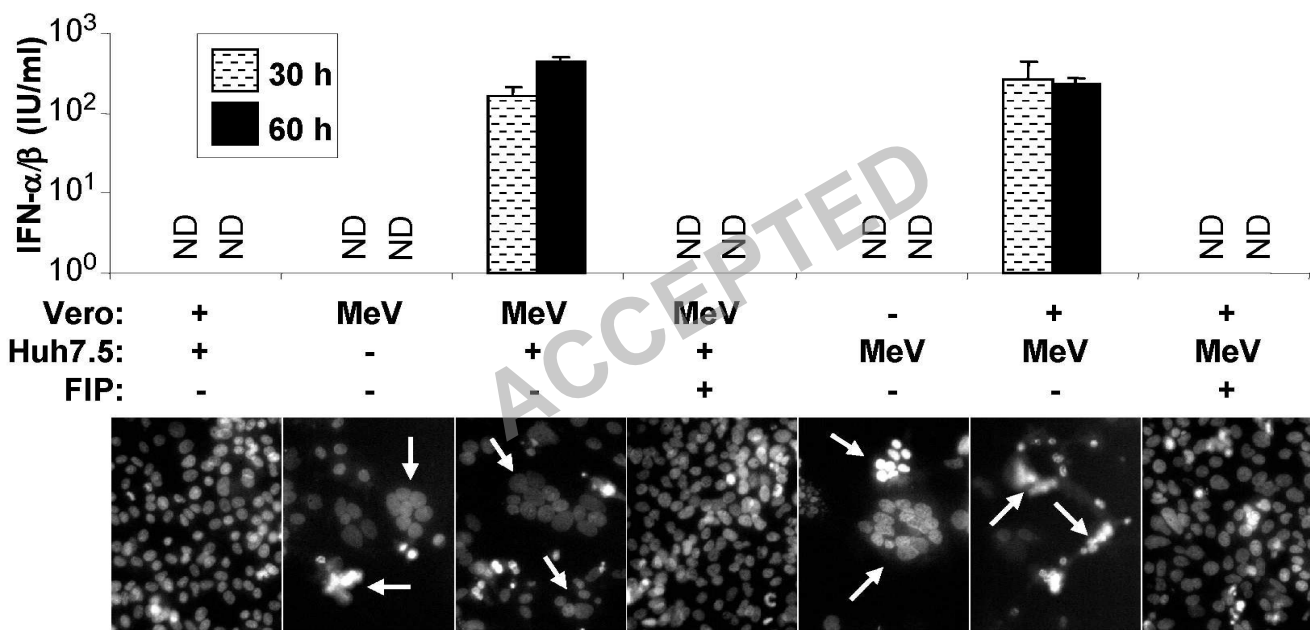


Figure 4

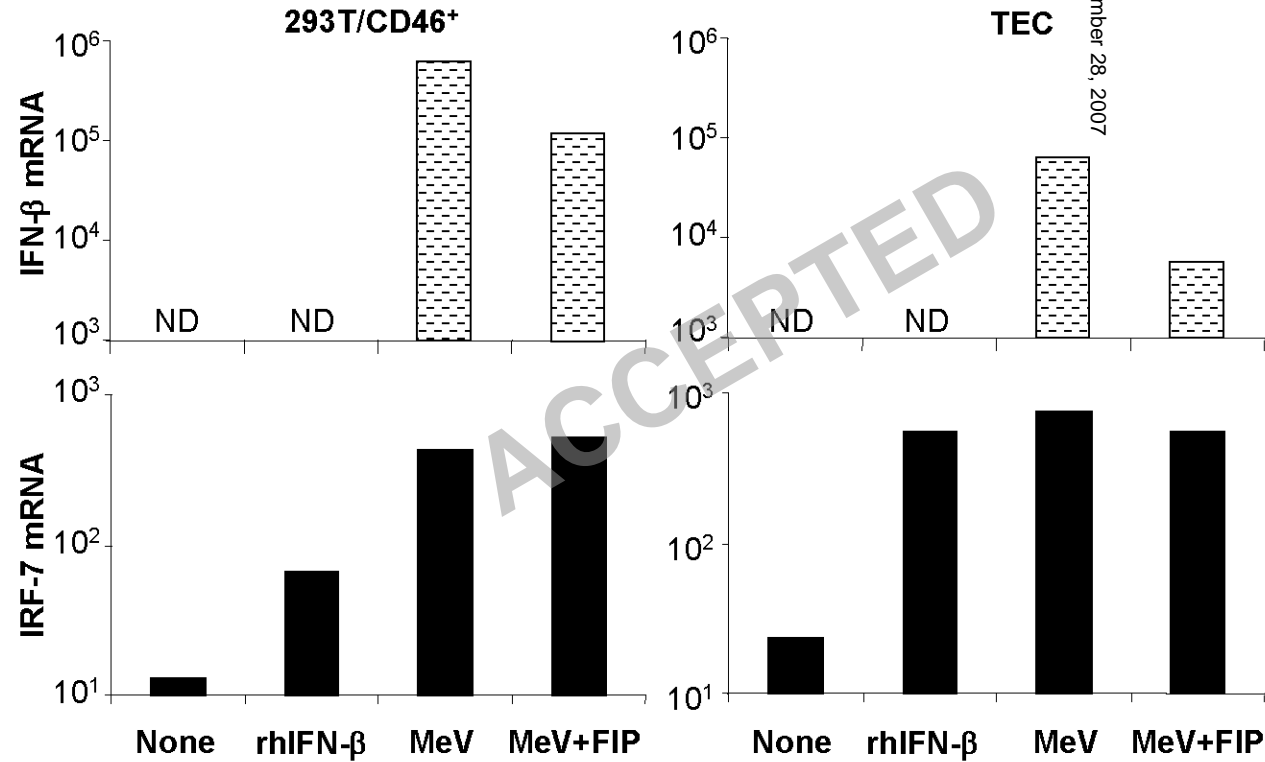
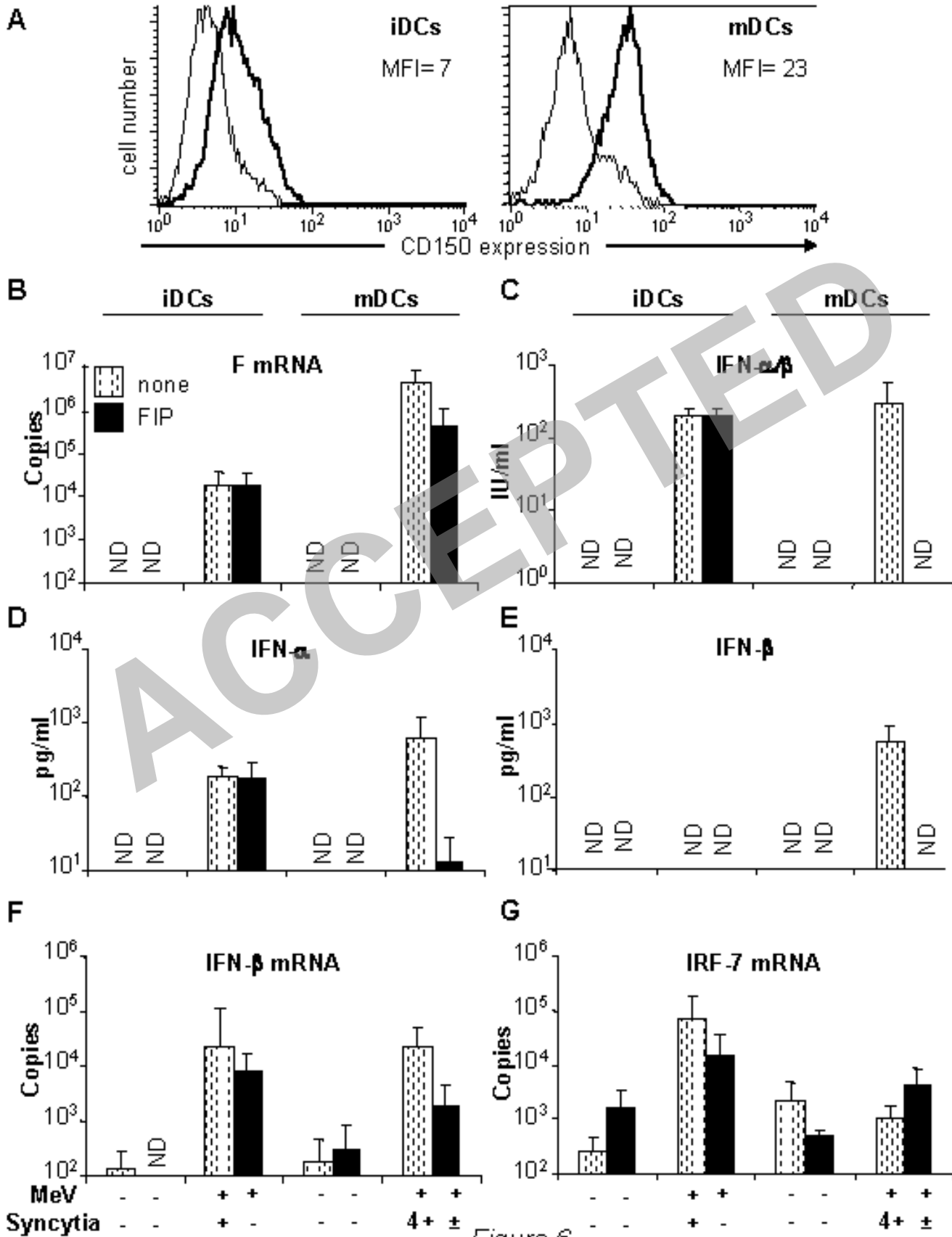


Figure 5



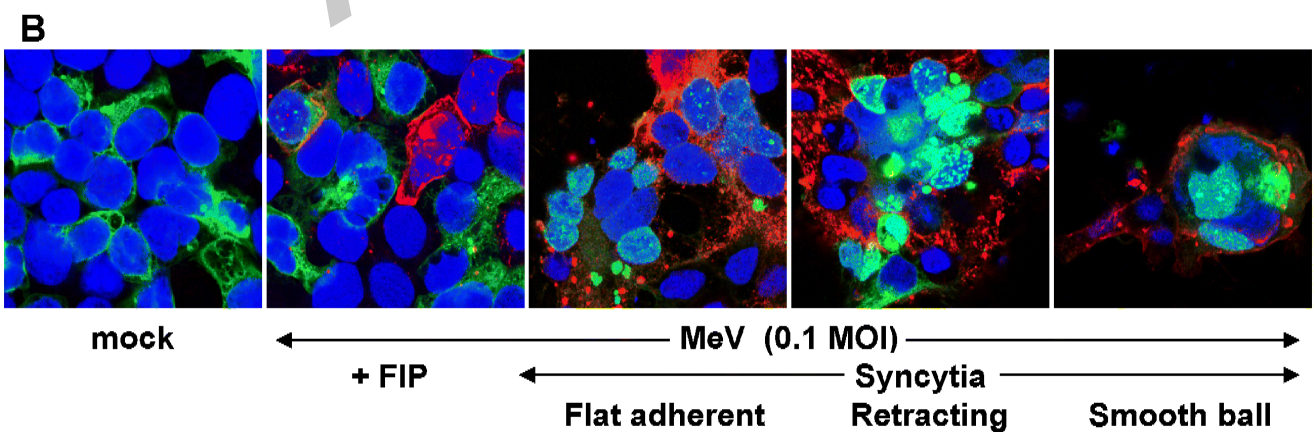
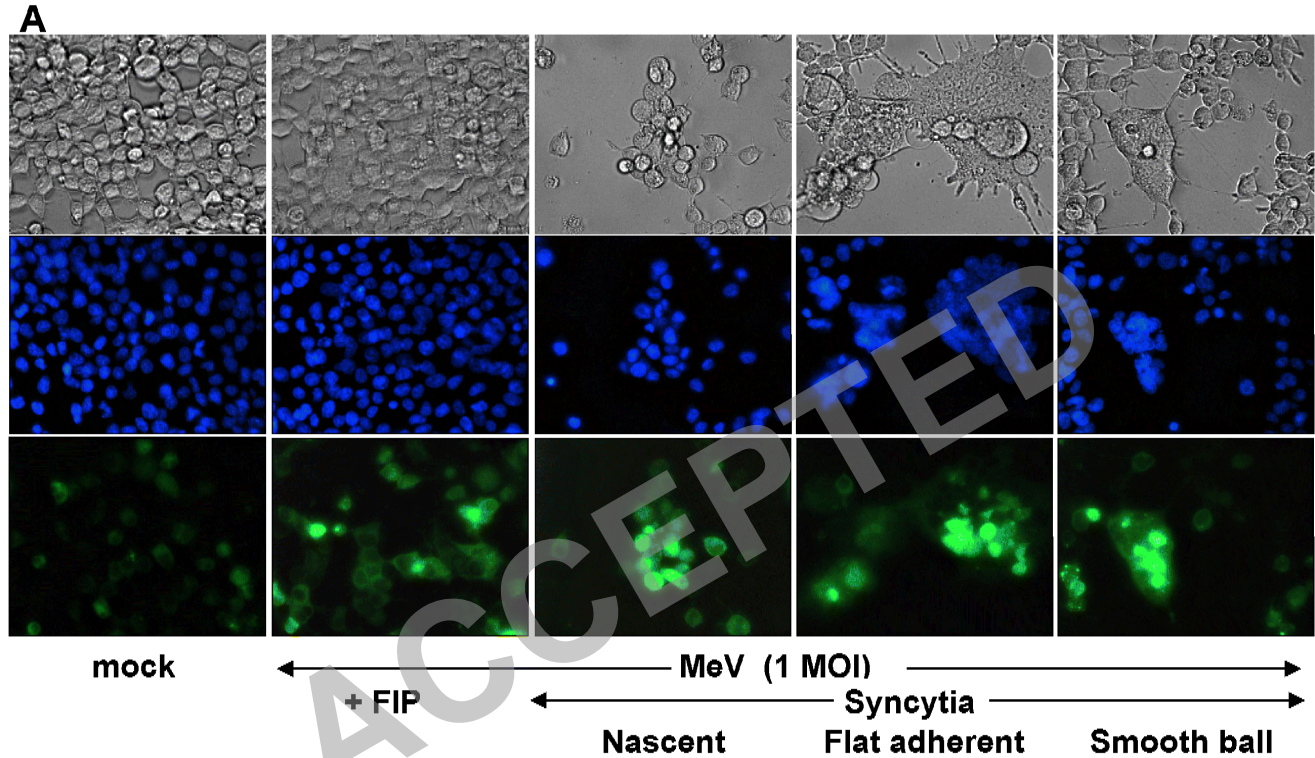


Figure 7 A,B

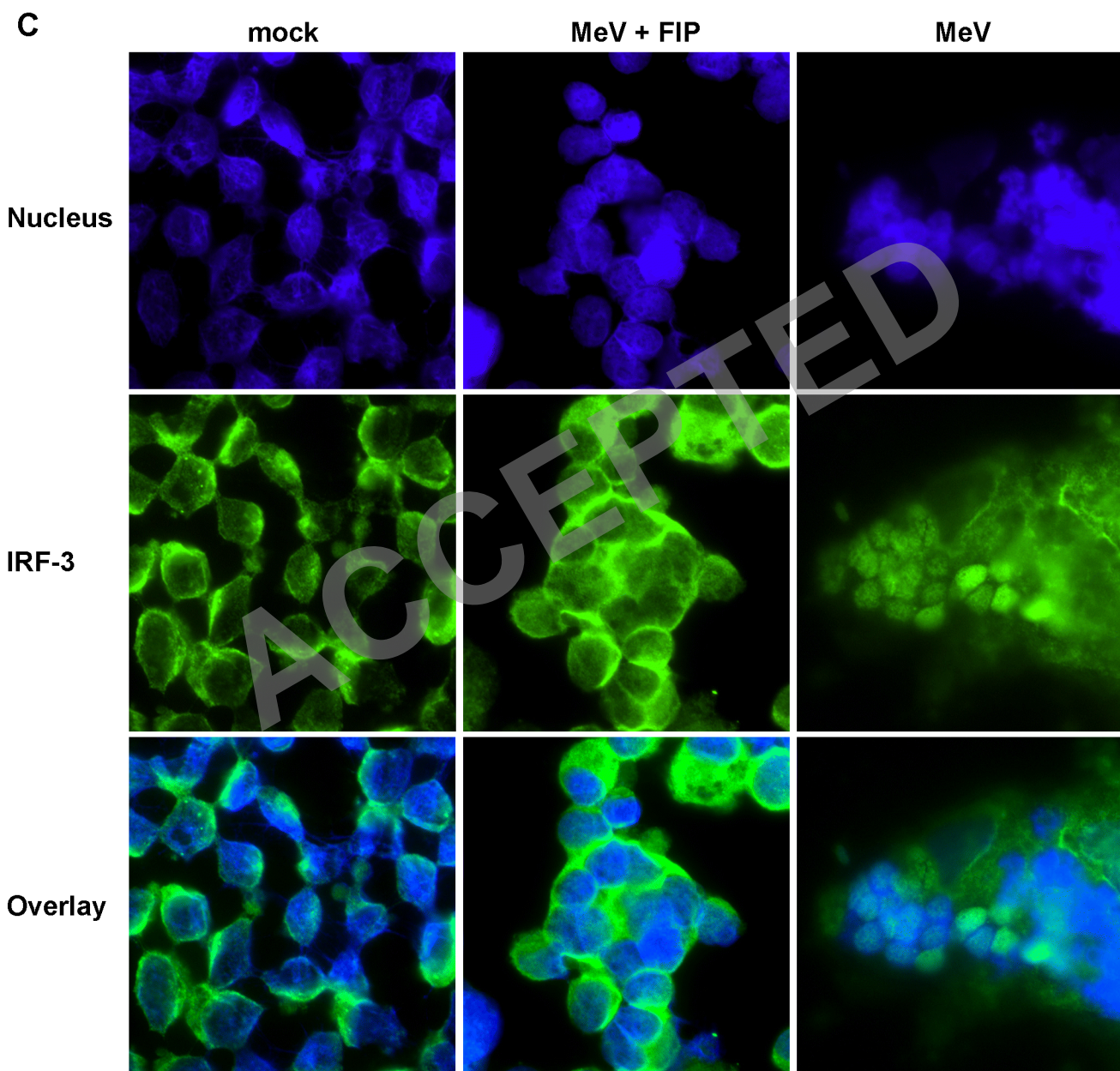


Figure 7C